Journal of Crystal Growth 312 (2010) 2154–2170

Contents lists available at ScienceDirect

Journal of Crystal Growth

journal homepage: www.elsevier.com/locate/jcrysgro

An experimental investigation of the columnar-to-equiaxed grain transition in aluminum–copper hypoeutectic and eutectic alloys

A.E. Ares [a,b,*], S.F. Gueijman [b], C.E. Schvezov [a,b]

[a] Member of CIC of the National Science Research Council of Argentina (CONICET)
[b] Professor of Faculty of Sciences, University of Misiones, 1552 Félix de Azara Street, 3300 Posadas-Misiones, Argentina

ARTICLE INFO

Article history:
Received 21 January 2010
Received in revised form
31 March 2010
Accepted 14 April 2010
Communicated by Prof. M. Rettenmayr
Available online 24 April 2010

Keywords:
A1. Directional solidification
A1. Columnar to equiaxed transition
A1. Dendrites
A1. Interphases
A2. Growth from melt
B1. Alloys

ABSTRACT

Providing benchmark data of the thermal and metallographic parameters during the columnar-to-equiaxed transition (CET) in a wide range of alloy concentrations is of fundamental importance for understanding this phenomenon as well as for metallurgical and modeling purposes. The aim of this study was to investigate the columnar-to-equiaxed transition (CET) in aluminum–copper alloys of different compositions covering a wide range from 2 to 33.2 wt%Cu (eutectic composition), which were directionally solidified from a chill face. The thermal parameters studied included recalescence, cooling rates, temperature gradients and interphase velocities. We found that the temperature gradient and velocity of the liquidus interphase reached critical values at the CET; these critical values were between −0.44 and 0.09 K/mm and between 0.67 and 2.16 mm/s, respectively. The metallographic parameters analyzed were grain size, primary and secondary dendritic arm spacing and also eutectic spacing. The results obtained were compared with previous experimental studies, published predictions and models of the CET for similar alloys.

1. Introduction

In general, as-cast alloys exhibit columnar grain structures that often end with an equiaxed zone, where the phenomenon of the columnar-to-equiaxed grain transition (CET) has taken place [1,2]. Since the grain structure influences the properties of a casting, a great deal of effort has been devoted in the last decades to understanding the mechanism behind the development of the macrostructure during solidification [3].

In particular in aluminum–copper alloys, Southin [4] reported that in diluted alloys (Al-0.1 and Al-2 wt%Cu) coarse dendrites that formed at the top of the ingot sinking into the melt play an important role in the formation of the alloy macrostructure. Morando et al. [5] examined the solidification of Al-2 wt%Cu cylindrical ingots by varying the volume from 5×10^4 to 5×10^6 mm^3 poured into graphite molds with a fixed ratio of internal diameter to internal height of 0.7. They obtained evidence that, with an increase in size, Southin's mechanism of equiaxed grain formation comes into play and that as solidification time increases crystal settling becomes more important [3]. Suri et al. [6] observed the CET in Al-4.5 wt%Cu alloys and reported that the CET occurred if $G<0.74v^{0.64}$, where G is the temperature gradient in the melt and v the tip growth rate.

Siqueira et al. [7] studied the CET in Al-2, Al-5, Al-8 and Al-10 wt%Cu alloys and found that the CET occurs on a nearly horizontal plane, at tip growth rates ranging from 0.28 to 0.88 mm s^{-1}, temperature gradients in the liquid ranging from 0.28 to 0.75 K mm^1 and critical cooling rate of 0.2 K s^{-1} [3]. Also, experiments conducted in Sn–Pb alloys have shown that a criterion should be based on a critical cooling rate of about 0.014 K/s, which depends only on the alloy system [8].

Gandin has published significant papers on CET and in his studies in Al–Si alloys, he determined negative gradients at the CET [9,10]; Browne [11], taking Al–Cu alloys as a case study, developed an equiaxed index for relative likelihood of CET, based on a front tracking model. His results were in agreement with the experimental findings of Siqueira et al. [7].

Hunt [12] developed a steady state directional solidification model for columnar and equiaxed growth of dendrites and eutectic alloys. The model was applied to Al-3 wt%Cu. The model predicts that at low growth velocities, equiaxed growth depends on the efficiency of the nucleating substrates for the equiaxed grains whereas at high gradients the number of nucleation sites is more important [3].

Ziv and Weinberg [13] using an unidirectional heat transfer model for the Al-3 wt%Cu alloy, determined that the CET occurred when the gradient fell to 0.06 K mm^{-1}, a result which is in agreement with a gradient prediction from Hunt solidification model [12].

* Corresponding author: 1552 Félix de Azara Street, (3300) Posadas-Misiones, Argentina. Tel.: +54 3752 422186x156; fax: +54 3752 425414.
E-mail address: aares@fceqyn.unam.edu.ar (A.E. Ares).

0022-0248/$ - see front matter © 2010 Elsevier B.V. All rights reserved.
doi:10.1016/j.jcrysgro.2010.04.040

Nomenclature

G temperature gradient
v tip growth rate
N the equiaxed grain density per unit volume [22,23]
ΔT_N undercooling at the heterogeneous nucleating temperature [12,22,23]
g_s grain size
λ_1 primary dendritic arm spacing
λ_2 secondary dendritic arm spacing
λ eutectic spacing
T_M melting temperature
T_L liquidus temperature
T_S solidus temperature
k partition coefficient
m_L liquidus slope
ρ_L density of the liquid phase
ρ_S density of the solid phase
C_L specific heat of the liquid phase
C_S specific heat of the solid phase
k_L thermal conductivity of the liquid phase
k_S thermal conductivity of the solid phase
α_L thermal diffusivity of the liquid phase
α_S thermal diffusivity of the solid phase
λ latent heat of fusion
σ_{SL} liquid/solid surface energy
D_L solute diffusivity
Γ Gibbs–Thomson coefficient
CET_{Min} minimum position of the CET
CET_{Max} maximum position of the CET
CET_{Ave} average position of the CET
CZ columnar zone
CET Z CET zone
EZ equiaxed zone
T_i temperature of thermocouple i
T_{i-1} temperature of thermocouple $i-1$
$T_{Liquidus}$ liquidus temperature
$T_{Solidus}$ solidus temperature
t_{SL} local solidification time
ΔT_U undercooling
ΔT_S superheating
ΔT_R recalescence
Δt_U nucleation (undercooling) time
Δt_S superheating time
Δt_R recalescence time
$\dot{T}$ cooling rate in K/s
G_i temperature gradients calculated from the readings of thermocouple i
G_L temperature gradient in the liquid
$G_{L(Critical)}$ value of the gradient at the moment of the CET
[liquid/(solid+liquid)] liquid interphase
[(solid+liquid)/solid] solid interphase
[solid+liquid] mushy zone
V_L liquidus interphase velocity
$V_{L(Critical)}$ value of the liquidus interphase velocity at the moment of the CET
ΔT is the error in temperature readings
Δx is the error of appreciation in distance
ΔG is the relative error in the measurement of the gradients
N_0 total number of heterogeneous substrate particles originally available per unit volume [12]
$\Delta T_C = \left(\frac{V' C_0}{A}\right)^{1/2}$ undercooling equal to that of the columnar growth front temperature [12]
V' is the real interface velocity [12]
A is a constant given by $A = \frac{1}{4\left(\frac{-2m_L(1-k)\Gamma}{D}\right)} = 300\,\frac{\mu m\%\text{weight}}{sK^2}$ for Al–Cu alloys
$\overline{\lambda}$ is the spacing of the lamellar structure [12]
$\overline{\lambda}_e$ is the average spacing of the lamellar structure [12]
$\phi_C \approx \frac{4\pi r_C^3 N_0}{3}$ is the equiaxed volume fraction
r_C is the maximum size of the equiaxed grains
$\Delta T_C = \left(\frac{V}{A}\right)^{1/2}$ is the fraction that is liquid behind the front
A is a constant equal to $27\,\frac{\mu m}{sK^2}$
B is a constant equal to 21.6 K μm
W is the width of the columnar grains
a is a fitting parameter which indicates the standard or absolute reference size for each concentration
b is a fitting parameter which indicates the degree of dependence of width with $\dot{T}$
C_0 alloy concentration
ε is a constant less than one. From experiences with different aluminum alloys, the value of $\varepsilon=0.5$ was adopted [36]
V_{TR} is the velocity of the cellular dendritic transition and is calculated as $V_{TR} = \frac{GD}{\Delta T_0 k}$, where $\Delta T_0 = -mC_0\frac{(1-k)}{k}$ [35]
ΔT is the range of solidification in nonequilibrium conditions $= \left(1 - \frac{GD}{V\Delta T_0}\right)\frac{\Delta T_0}{(1-k)}$ [35]
L is a constant [32–34]

Gäumann et al. [14] developed a numerical model as a modification of Hunt's solidification model [11] and argued that the model is more appropriate for predicting the CET in a range of processes, including the high cooling rates experienced in welding and rapid solidification processes.

Zhu and Smith [15] developed an improved Monte Carlo model, by removing some of the limitations of the model reported by Brown and Spittle [16]. The model was applied to the prediction of the multidirectional freezing of a 2D ingot of Al-4.5 wt%Cu.

Dong and Lee [17] utilized a CA–FD model to simulate the CET by modeling the solidification of an Al-3 wt%Cu alloy with $G=3\ \text{K mm}^{-1}$ and V varying as a function of the solidification time to give values similar to those in the non-steady studies of Ares and Schvezov [18,19] and Siqueira et al. [7].

McFadden et al. [20] compared four models developed to predict the CET. They calculated that three of the indirect methods based on the following criteria; constrained-to-unconstrained transition [10], the critical cooling rate [7,8] and the peak equiaxed index [11] may be used in conjunction with the columnar-front-tracking model to predict the CET position in noninoculated directional castings.

Mathiesen et al. [21] analyzed by synchrotron X-ray video microscopy the crystal fragmentation and columnar-to-equiaxed transition in Al-20 and Al-30 wt%Cu alloys. They concluded that buoyant forces are responsible for the transport of fragments out of the mush in a manner that would cause macro and mesoscale segregation rather than CET in a nonconfided 3D mold.

Also, Nguyen-Thi et al. [22] and Reinhart et al. [23] realized in situ and real-time investigation of columnar-to-equiaxed transition in Al-3.5 wt%Ni alloy at the European Synchrotron Radiation Facility (ESRF). They analyzed the dendritic morphologies as a function of the solidification parameters during

columnar growth (low pulling rates) and equiaxed growth (high pulling rates) and concluded that the solutal undercooling ahead of the columnar front increases when increasing the pulling rates, consequently, a broader range of particles become active. Also, that the equiaxed grain density per unit volume, N, is one of the key parameters for CET and equiaxed growth. They obtained N directly by measuring the size of the equiaxed grains soon after their capture by the eutectic front. They estimated an experimental value of $N_{max}=1.25\times10^5\ cm^{-3}$ and used this value to obtain a Hunt's CET diagram, with $\Delta T_N=0.1$ K. The experimental points of fully equiaxed growth and elongated grains fall in the mixed columnar-equiaxed region, as defined by Hunt [12].

While all these works have significantly contributed from different aspects to understanding the phenomenon of the CET, there are no sufficient data in the literature about detailed measurements of thermal and metallographic parameters in a wide range of concentrations of different specific alloy systems, including eutectic composition.

The objective of the present work was to generate detailed experimental data of thermal (cooling rate, temperature gradient, recalescence, solidification velocity) and metallographic (grain size, primary and secondary dendritic spacings and eutectic spacing) parameters during directional solidification of aluminum–copper hypoeutectic (Al-2, Al-4, Al-10, Al-20 wt%Cu) and also eutectic (Al-33.2 wt%Cu) alloys with the CET and finally correlate metallographic with thermal parameters in each zone of the samples (columnar, CET and equiaxed).

2. Experimental procedure

The alloy samples were melted and solidified directionally upwards in an experimental setup detailed in previous articles [18,19]. The temperature measurements were performed using K-type thermocouples protected with ceramic shields and connected to a data acquisition system controlled by a computer.

The thermocouples were previously calibrated using four temperature points: the freezing and boiling points (corrected by atmospheric pressure) of demineralized water and the melting points of aluminum (99.999 wt%) and copper (99.9999 wt%). The accuracy of the thermocouples was determined to be between ±0.25 K. The samples were melted in alumina molds of 23 mm i.d. and 25 mm e.d., with a flat bottom and a 200-mm-high cylindrical uniform section.

Five thermocouples were positioned at 20-mm intervals on the centerline of the cylinder mold from the bottom surface of the mold. During a solidification experiment, the temperature measured by each thermocouple was recorded at regular intervals of time. Different intervals were previously tested, and as a result of this exercise, an interval of 1 s was selected. For the data processing, the readings made every 0.10 s for 1 s were averaged, and this value was associated with the middle of the averaged interval. This procedure was chosen as a result of a compromise between the memory available in the data logger, the time taken for an entire solidification experiment, and the degree of precision to capture the main phenomena occurring during the CET.

The experimental procedure was as follows. At first, the liquid metal inside the mold in the furnace was allowed to reach the selected temperature: once a uniform temperature was reached, less than 1 K of difference recorded between the five thermocouples located at different positions in the melt, the furnace power was turned off and the melt was allowed to solidify from the bottom.

Heat was extracted through a cooling system, which consisted of a copper disk attached to a copper coil, both cooled by running water. The solidification velocity was adjusted by changing the temperature and water flow and by adding plates of materials between the copper plate and the crucible, which changed the effective value of the thermal conductivity.

The crucible was also isolated on the top to reduce heat losses from the top of the furnace to a minimum. Temperature data acquisition was started approximately at the same time at which the furnace power was turned off in order to record the entire unidirectional solidification process. The measurements showed that the initial temperature (superheat) ranged from 1353.2 to 933.6 K in all the experiments. With this experimental setup, unidirectional heat flow was achieved and the convection associated with the pouring of the liquid into the mold was eliminated.

After directional solidification, the cylindrical ingots were cut on a mid longitudinal plane. Then, the samples were polished with sand paper and the samples with less than 10 wt%Cu were etched with a solution containing 15 ml HF, 4.5 ml HNO_3, 9.0 ml HCl and 271.5 ml H_2O. The samples with 20 wt%Cu and 33.2 wt%Cu were etched with a solution containing 320 ml HCl, 160 ml HNO_3 and 20 ml HF. Etching was performed at room temperature [24]. The position of the transition was located by visual observation and optical microscopy, and the distance from the bottom of the sample was measured with a ruler, see Fig. 1(a) and (e).

The microstructure was analyzed using Scanning Electron Microscopy (SEM) and an inverted metallographic microscope (Arcano XTL 3400). The equiaxed grain size (g_s) was measured, at equally spaced intervals, starting at the position where the transition began, utilizing the ASTM E112 standard norm [25] and a typical histogram showing the frequency of the size of the equiaxed grains for each sample. The columnar region was divided in a similar way and the width and length of the grains measured directly.

In each zone of the directional solidified samples (columnar, equiaxed and CET), the primary (λ_1) and secondary (λ_2) dendritic arm spacing and the eutectic (λ) spacing were measured in cross sections of one half of each sample (Fig. 1(b–d) and (f–h)). Each section was mounted, polished and etched with 1 g NaOH and 100 ml H_2O for 5–15 s at room temperature and the spacings were determined in columnar, CET and equiaxed zones by the number of interception in a straight line. Twenty values of spacings were measured for each position. As an example, in Fig. 1(b) and (c), no. (1) is indicating the position of the primary arm spacing and no. (2) the position of secondary dendritic arm spacing. In equiaxed growth, primary spacing was defined and measured as the distance between the centers of the equiaxed dendrites; see Fig. 1(d). The center of the equiaxed dendrite is indicated by no. (1). Also, the secondary arm spacing is represented by no. (2).

3. Results and discussion

The results presented and discussed here are related to the characterization of: (1) the columnar-to-equiaxed transition (CET); (2) the thermal parameters involved (recalescence, cooling rate, temperature gradient and solidification velocity); (3) the metallographic parameters measurements (grain size, primary and secondary dendritic and eutectic spacings) and (4) relation of the size of metallographic parameters with the calculated thermal parameters in each zone of the samples (columnar, CET and equiaxed).

Twenty-five experiments in a range of alloy composition and cooling rate were performed. The alloys prepared were Al-2, Al-4, Al-10, Al-20 and Al-33.2 wt%Cu (eutectic composition).

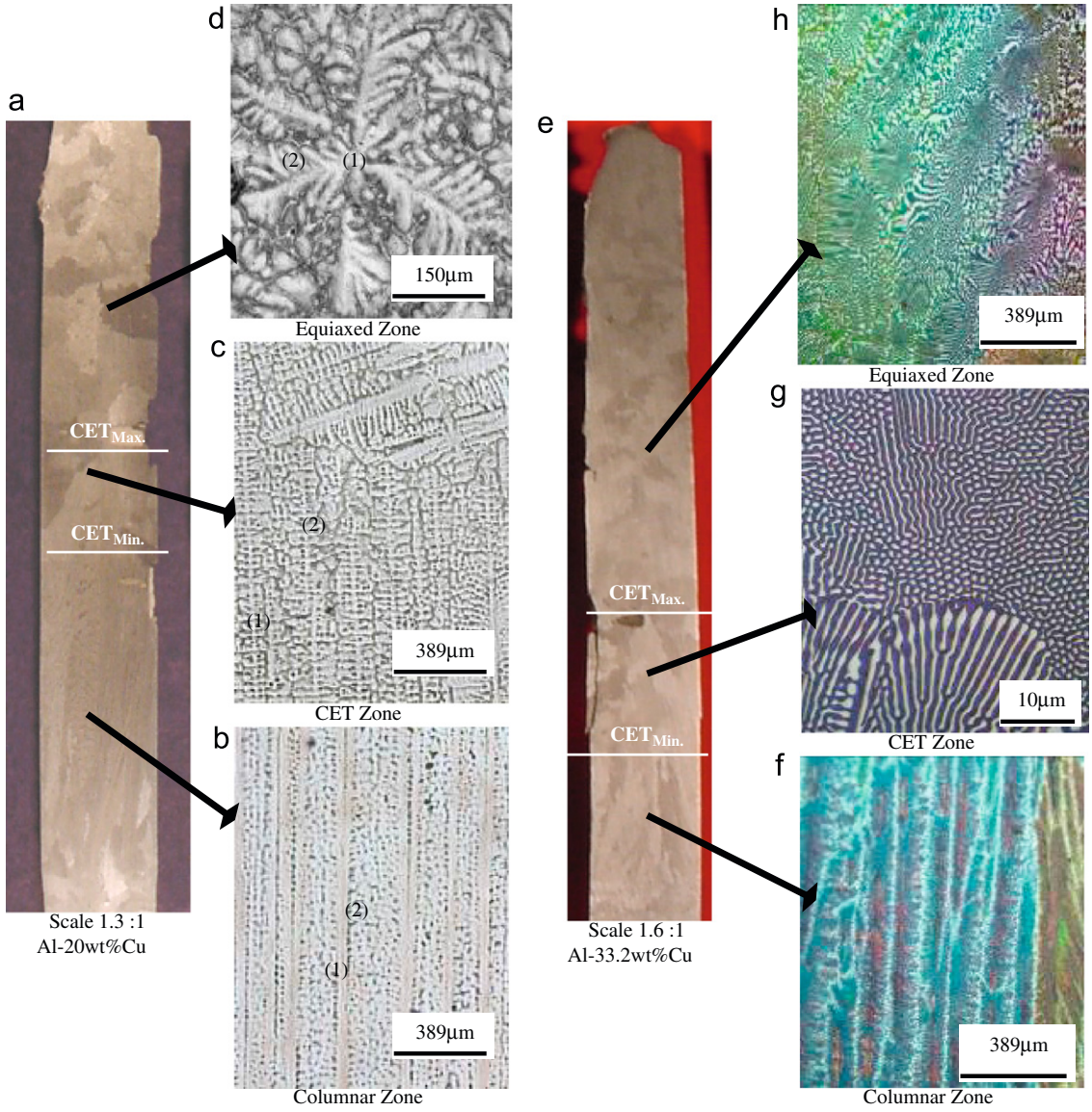

Fig. 1. (a) Macrostructure of the Al-20 wt%Cu alloy. (b–d) Microstructures of the columnar, CET and equiaxed zones of the same sample (As an example, in the three microstructures no. (1) is indicating the position of the primary spacing and no. (2) the position of secondary dendritic spacing). The primary spacing in the equiaxed zones of the samples is measured as the distance between centers of the dendrites (no. (1) in Fig. (d)). (e) Macrostructure of the Al-33.2 wt%Cu alloy. (f–h) Representative microstructures of each zone of the eutectic sample showing the lamellar and rod-like shapes.

Table 1
Thermophysical properties of aluminum–copper alloys [25,47–49].

Property data	Al	Cu	Al-2 wt%Cu[a]	Al-4 wt%Cu[a]	Al-10 wt%Cu[a]	Al-20 wt%Cu[a]	Al-33.2 wt%Cu[a]
Melting temperature, T_M (K)	933	1356	–	–	–	–	–
Liquidus temperature, T_L(K)	–	–	928	923	906	873	821
Solidus temperature, T_S (K)	–	–	894	851	821	821	821
Partition coefficient, k	–	–	0.17	0.17	0.17	0.17	0.17
Liquidus slope, m_L (K wt%)	–	–	−2.6	−2.6	−2.6	−2.6	–
Density of the liquid phase, ρ_L (kg/m^3)	2380	8447.0	2501.3	2622.6	2986.7	3593.4	4394.2
Density of the solid phase, ρ_S (kg/m^3)	2550	8956.2	2678.1	2806.2	3190.6	3831.2	4507.8
Specific heat of the liquid phase, C_L (J/kg K)	1086	505.9	1074.4	1062.8	1027.9	969.9	893.4
Specific heat of the solid phase, C_S (J/kg K)	1123	384.2	1108.2	1093.4	1049.1	975.2	872.1
Thermal conductivity of the liquid phase, k_L (W/mK)	92	334.3	96.8	101.7	116.2	140.5	172.4
Thermal conductivity of the solid phase, k_S (W/mK)	222	398.9	225.5	229.1	239.7	257.4	280.7
Thermal diffusivity of the liquid phase, α_L (m^2/s)	3.36×10^{-5}	3.44×10^{-5}	4.18×10^{-5}	4.16×10^{-5}	4.12×10^{-5}	4.05×10^{-5}	3.95×10^{-5}
Thermal diffusivity of the solid phase, α_S (m^2/s)	7.75×10^{-5}	1.11×10^{-4}	9.43×10^{-5}	9.47×10^{-5}	9.57×10^{-5}	9.74×10^{-5}	9.96×10^{-5}
Latent heat of fusion, λ (kJ/kg)	396	205	392.2	388.4	376.9	357.8	332.6
Liquid/solid surface energy, σ_{SL} (J/m^2)	–	–	169×10^{-3}	169×10^{-3}	169×10^{-3}	169×10^{-3}	169×10^{-3}
Solute diffusivity, D_L (m^2/s)	–	–	3.5×10^{-9}	3.5×10^{-9}	3.5×10^{-9}	3.5×10^{-9}	3.5×10^{-9}
Gibbs–Thomson coefficient, Γ (mK)	–	–	2.41×10^{-7}	2.41×10^{-7}	2.41×10^{-7}	2.41×10^{-7}	2.41×10^{-7}

[a] Calculated.

The thermophysical properties of these alloys are presented in Table 1.

3.1. Columnar-to-equiaxed transition (CET) in dendritic and eutectic alloys

The CET can be observed in Fig. 1(a) for Al-20 wt%Cu and (e) for Al-33.2 wt%Cu. First of all, no effect of the set of thermocouples in the transition was observed; either acting as nucleating sites or changing the solidification structure. From the macrographs in Fig. 1(a) and (e), it is possible to appreciate that the transition in grain size is not sharp. The distances of initiation (CET_{Min}) and ending (CET_{Max}) of the transition and the average position of the CET ($CET_{Average}$), are shown for each alloy in Table 2. Similarly, Vandyoussefi and Greer obtained that the CET is gradual in Al-4.15 wt%Mg alloys [26]. Ares and Schvezov reported observations of CET in Pb–Sn [18] and Zn–Al [19] alloys indicating that the transition occurs in a region where both kinds columnar and equiaxed grains co-exist and that in no case the columnar growth is restored. On the other hand, Ziv and Weinberg observed that the CET in Al-3 wt%Cu occurred relatively abruptly, on a near horizontal plane [13], whereas Gandin found that the CET is sharp [9,10], and Siqueira et al. [7,8] obtained results similar to those of Ziv and Weinberg in Al-2, Al-5, Al-8 and Al-10 wt%Cu. The results obtained by Martorano et al. [27] were in complete agreement with the experimental macrographs of Gandin [9].

The typical microstructures of solidification in the three regions, columnar, transition and equiaxed, for two compositions, Al-20 and Al-33.2, are shown in Fig. 1(b–d) and (f–h), respectively. In Fig. 1(b–d), the microstructure is dendritic, and in (f–h), the microstructure is lamellar and rod-like.

The results of the present investigation show that there is also a transition from the columnar to the equiaxed type of solidification at the eutectic concentration, 33.2 wt%Al (Fig. 1(e)); the columnar type of growth is characterized by different grains along the direction of heat extraction, each presenting a mixed structure of lamellar and rod-like shapes, and both the grains and the lamellae are oriented in the direction of heat extraction (Fig. 1(f)). The transition region presents characteristics similar to those of the lower concentrated alloys, with grains with no preferred equiaxed orientation and with lamellar rod-like eutectic structures coexisting with columnar grains (Fig. 1(g)). The equiaxed region presents smaller equiaxed grains with a finer lamellar structure at the center of the grains and a coarser rod-like structure at the grain periphery. This could be indicating a different thermal behavior at the periphery of the sample with respect to the center, which is significant enough to produce a different eutectic structure in each region.

3.2. Characterization of the thermal parameters

3.2.1. Temperature versus time curves

A typical set of cooling curves is shown in Fig. 2(a) and (c) utilizing four thermocouples. The thermocouple T_1 is at the lowest position and is the first to reach the solidification front, whereas T_4 is at the highest position. In all the curves it is possible to identify a period corresponding to the cooling of the melt, a second period of solidification and a final period of cooling of the solid to ambient temperature.

3.2.2. Recalescence

In the experiments where the transition occurs, an effect of recalescence is normally observed [2,18,28]. The characteristics of this observation can be described using the insets of Fig. 2.

Table 2
Alloy composition used in the experiments and observations: average cooling rate, $\dot{T}$, minimum CET position, CET_{Min}, maximum CET position, CET_{Max}, average CET position, $CET_{Average}$, liquidus interphase velocity at the CET instant, $V_{L\ (Critical)}$, temperature gradient at the CET instant, $G_{L(Critical)}$, and average values of these parameters for each alloy concentration.

#	Alloy wt%Cu	$\dot{T}$ (K/s)	CET_{Min} (mm)	CET_{Max} (mm)	CET_{Ave} (mm)	$V_{L(Critical)}$ (mm/s)	$G_{L(Critical)}$ (K/mm)	Averages values of parameters for each composition
1	Al-2 wt%Cu	2.1	43.5	66.9	55.2	1.45	−0.38	$\dot{T}_{Ave} = 1.6$ K/s
2		1.8	38.1	50.8	43.5	1.82	−0.16	CET_{Ave}=39.2 mm
3		1.1	18.0	38.8	28.4	0.83	−0.06	$V_{L(Critical)=}$1.16 mm/s
4		1.4	21.0	33.6	27.3	0.67	0.09	$G_{L(Critical)}$= −0.134 K/mm
5		1.6	34.0	49.0	41.5	1.04	−0.15	
6	Al-4 wt%Cu	1.7	37.0	48.5	43.3	1.28	−0.05	$\dot{T}_{Ave} = 1.7$ K/s
7		1.6	32.0	46.6	39.3	0.95	0.01	CET_{Ave}=40.0 mm
8		2.2	40.5	77.9	56.7	1.43	−0.19	$V_{L(Critical)=}$1.25 mm/s
9		1.3	20.9	34.3	27.6	1.11	0.08	$G_{L(Critical)}$= −0.018 K/mm
10		1.5	22.7	43.5	33.1	1.5 1	0.06	
11	Al-10 wt%Cu	2.4	55.0	74.4	64.7	1.64	−0.16	$\dot{T}_{Ave} = 2.0$ K/s
12		2.3	50.0	73.8	62.9	1.59	−0.13	CET_{Ave}=54.4 mm
13		1.6	30.5	42.9	36.7	1.16	0.05	$V_{L(Critical)}$=1.46 mm/s
14		1.8	39.0	54.0	46.5	1.33	0.04	$G_{L(Critical)}$= −0.06 K/mm
15		2.1	38.3	71.9	61.1	1.61	−0.10	
16	Al-20 wt%Cu	2.4	56.9	75.1	66	1.79	−0.14	$\dot{T}_{Ave} = 2.1$ K/s
17		1.9	39.6	62.4	52	1.49	0.01	CET_{Ave}=58.6 mm
18		2.0	36.4	76.8	55.6	1.72	−0.12	$V_{L(Critical)}$=1.68 mm/s
19		1.7	31.5	52.5	44	1.34	0.07	$G_{L(Critical)}$= −0.106 K/mm
20		2.7	66.8	84.4	75.6	2.08	−0.35	
21	Al-33.2 wt%Cu	2.6	53.7	74.9	64.3	2.16	−0.44	$\dot{T}_{Ave} = 2.2$ K/s
22		2.9	54.0	75.2	64.6	1.97	−0.17	CET_{Ave}=49.1 mm
23		2.2	34.0	74.6	54.3	1.87	−0.12	$V_{L(Critical)}$=1.86 mm/s
24		1.7	28.0	40.0	34	1.62	0.00	$G_{L(Critical)}$= −0.156 K/mm
25		1.5	16.0	41.0	28.5	1.71	−0.05	

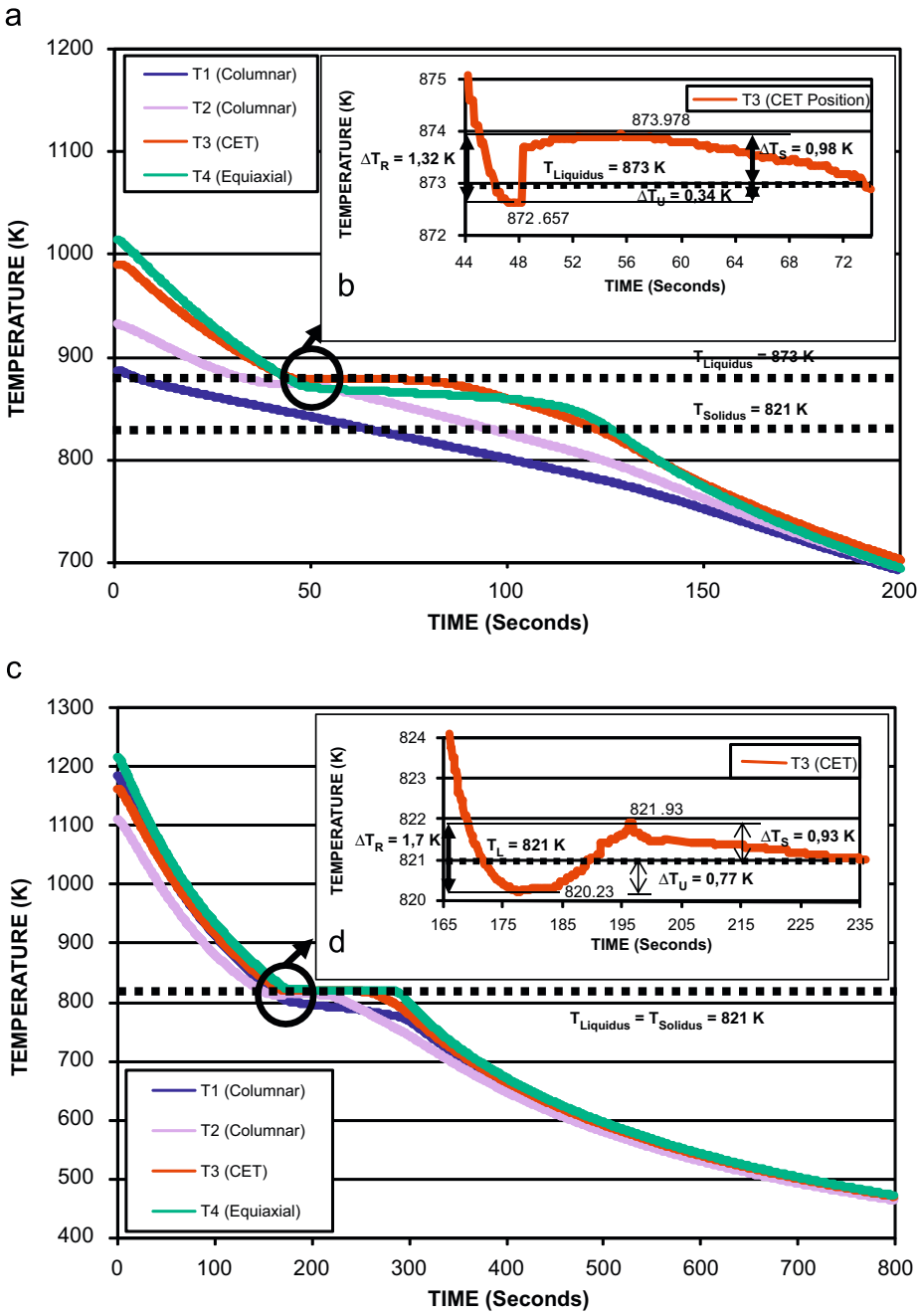

Fig. 2. Cooling curves for two different experiences. (a) and (b) Al-20 wt%Cu, (c) and (d) Al-33.2 wt%Cu. Figs. (b) and (d) represent an enlargement of a short period of time of a region of Figs. (a) and (c), respectively.

Fig. 2(b) and (d) represents an enlargement of a short period of time of a region in Fig. 2(a) and (c), respectively, which corresponds to the CET zone, for thermocouple T_3 measured during both experiments with Al-20 and Al-33.2 wt%Cu.

It is noteworthy to point out that after the start of the transition, there is a slight increase in the temperature above the plateau (superheating, ΔT_S), after reaching a minimum value below the liquidus temperature, $T_{Liquidus}$ (undercooling, ΔT_U). This recalescence, ΔT_R, ($\Delta T_R = \Delta T_U + \Delta T_S$) lasts for only a few seconds (between 7 and 26 s, depending on the composition of the alloy); however, the region affected could be longer than the separation between thermocouples (20 mm).

The nucleation time (or undercooling time), Δt_U, is defined as the time when the nucleus of solid appears in the melt, between $T_{Liquidus}$ and the minimum value of temperature below the liquidus temperature. Comparing the behavior in relation to the alloy concentration, it is observed that for the Al-20 wt%Cu alloy, the nucleation time is about 4 s, much shorter than for the eutectic alloy, which is around 15 s. The superheating time, Δt_S, is defined as the time when there is a diffusion of the latent heat above the $T_{Liquidus}$, when the nucleus started to grow. The superheating time is about 3 s for Al-20 wt%Cu alloy and 11 s for Al-33.2 wt%Cu alloy.

The average values of undercooling, ΔT_U, and superheating, ΔT_S, show that both increase with alloy concentration; in the first case, it increases from 0.33 to 0.64 K, whereas in the second, it increases from 0.37 to 1.06 K. The added value of recalescence $\Delta T_R = \Delta T_U + \Delta T_S$ also increases from 0.79 to 1.65 K. Also, the time involved in each step, that is, Δt_U, Δt_S and Δt_R, is shown in Table 3.

Table 3
Measured values of undercooling, ΔT_U, superheating, ΔT_S, and recalescence, ΔT_R, in the position of the CET thermocouple for each experiment, the corresponding interval of time involved (Δt_U, Δt_S and Δt_R) and average values of each.

#	Alloy wt%Cu	ΔT_U (K)	Δt_U (S)	Average values of ΔT_U and Δt_U	ΔT_S (K)	Δt_S (S)	Average values of ΔT_S and Δt_S	ΔT_R (K)	Δt_R (S)	Average values of ΔT_R and Δt_R
1	Al-2 wt%Cu	0.37	2.36		0.55	3.79		0.92	6.15	
2		0.33	1.84	ΔT_U=0.33 K	0.47	3.61	ΔT_S=0.37 K	0.80	5.45	ΔT_R=0.79 K
3		0.31	4.46	Δt_U=3.06 s	0.42	4.62	Δt_S=4.71 s	0.73	9.08	Δt_R=7.77 s
4		0.29	1.57		0.38	2.25		0.67	3.82	
5		0.34	5.09		0.53	9.27		0.87	14.36	
6	Al-4 wt%Cu	0.35	1.61		0.53	6.42		0.88	8.03	
7		0.33	3.44	ΔT_U=0.34 K	0.57	10.46	ΔT_S=0.54 K	0.90	13.9	ΔT_R=0.87 K
8		0.37	2.13	Δt_U=2.802 s	0.65	11.93	Δt_S=7.93 s	1.02	14.06	Δt_R=10.73 s
9		0.30	1.55		0.44	4.37		0.74	5.92	
10		0.34	5.28		0.48	6.44		0.82	11.72	
11	Al-10 wt%Cu	0.49	8.12		0.87	13.24		1.36	21.36	
12		0.44	4.96	ΔT_U=0.45 K	0.88	11.09	ΔT_S=0.84 K	1.32	16.05	ΔT_R=1.29 K
13		0.41	5.14	Δt_U=5.73 s	0.75	14.37	Δt_S=14.01 s	1.16	19.51	Δt_R=19.75 s
14		0.43	6.97		0.82	17.46		1.25	24.43	
15		0.46	3.48		0.89	13.92		1.35	17.40	
16	Al-20 wt%Cu	0.34	1.59		0.98	7.8		1.32	9.39	
17		0.55	7.08	ΔT_U=0.52 K	0.83	5.6	ΔT_S=0.90 K	1.38	12.68	ΔT_R=1.39 K
18		0.67	4.25	Δt_U=5.38 s	0.92	10.13	Δt_S=11.06 s	1.46	14.38	Δt_R=19.75 s
19		0.37	6.42		0.80	14.70		1.17	21.12	
20		0.69	7.56		0.98	17.08		1.61	24.64	
21	Al-33.2 wt%Cu	0.77	6.04		0.93	18.18		1.70	24.22	
22		0.69	2.21	ΔT_U=0.64 K	1.04	21.81	ΔT_S=1.06 K	1.73	24.02	ΔT_R=1.65 K
23		0.61	8.73	Δt_U=6.55 s	1.01	20.54	Δt_S=20.79 s	1.62	29.27	Δt_R=26.54 s
24		0.57	5.46		1.09	23.14		1.66	28.60	
25		0.57	10.31		0.96	20.28		1.53	30.59	

In all the cases, the time implicated increases with the increase in alloy concentration.

3.2.3. Cooling rates

The cooling rate, $\dot{T}$, was determined from the temperature versus the time curves at each thermocouple position and taking the average slope during the cooling of the melt, before a period of solidification. The temperature interval utilized to calculate the slope was between the liquidus temperature and the highest temperature above the liquidus reached by the melt before the furnace was turned off.

Comparing the cooling rates with the distances, which correspond to the length of the columnar zone, for all alloys, it is observed that as the cooling rate increases the length of the columnar grains increases as well. This is possible by comparing the results of experiments 1–5 for Al-2 wt%Cu, with values of cooling rates of 1.1, 1.4, 1.6, 1.8 and 2.1 K/s, which result in minimum columnar zones of 18, 21, 34, 38.1 and 43.5 mm, respectively (see Table 2).

In order to determine the effect of alloy composition on the length of the columnar zone, it is necessary to consider the results obtained with the same cooling rates in Table 2. If we compare the results of experiment # 5 for Al-2 wt%Cu, experiment # 7 for Al-4 wt%Cu and experiment # 13 for Al-10 wt%Cu, with approximately similar cooling rates (1.6 K/s), which result in minimum columnar zones of 34.0, 32.0 and 30.5 mm, respectively, increasing the aluminum content produces smaller columnar zones at a given cooling rate. This result agrees with other previously reported experimental results [9–10,13,29–31].

3.2.4. Temperature gradients

The temperature gradients at all times were calculated straightforward, dividing the temperature difference between the two thermocouples by the separation distance between them.

The error in the temperature readings, considering the average procedure and the sensitivity of the data logger in the digital process, is ΔT=0.25 K. In the case of the distance between thermocouples, the error of appreciation is Δx=1 mm, from which the relative error in the measurement of the gradients results to be $\Delta G = \frac{G}{T_{i-1}-T_i} + 0.05G$, where a separation between thermocouples of 20 mm was used.

The temperature gradients calculated from the readings of five thermocouples for Al-2 wt%Cu are presented in Fig. 3. They are referred as G_1, G_2, G_3 and G_4. The period of time is 300 s (5 min), which comprises the whole solidification process including the transition. The vertical lines in Fig. 3 show the time at which the liquidus front reaches each thermocouple position; line T_1 coincides with the vertical axis and corresponds to the origin of the time axis.

In 59.25 s the liquidus front reaches the T_2 thermocouple position. In 90.64 s the liquidus front reaches the T_3 thermocouple position, which is the time when the transition at T_3 occurs. At the beginning the gradients in the liquid measured from thermocouples T3 and T4 where the alloy is liquid are larger, with values around 6 °C/cm at the bottom of the sample, and 23 °C/cm at the top. When the transition occurs, these values gradually decrease, and the temperature gradient in the liquid becomes small and slightly negative, about −0.162 K/mm in this case; this is the value of the critical temperature gradient in the liquid, $G_{L(Critical)}$, for this experiment. After this, the gradients increase during the final cool down of the solid. A similar behavior can be observed in all the samples. The critical temperature gradients in the liquid for all the experiments are listed in Table 2. The scatter in the values of the gradient is associated with the fact that the transition usually occurs between two thermocouples and therefore, the calculated value is an average over a region which includes the mushy zone and the melt. In addition, according to the relative error presented above, at these low values of temperature differences, the error in the calculated gradients could be as large

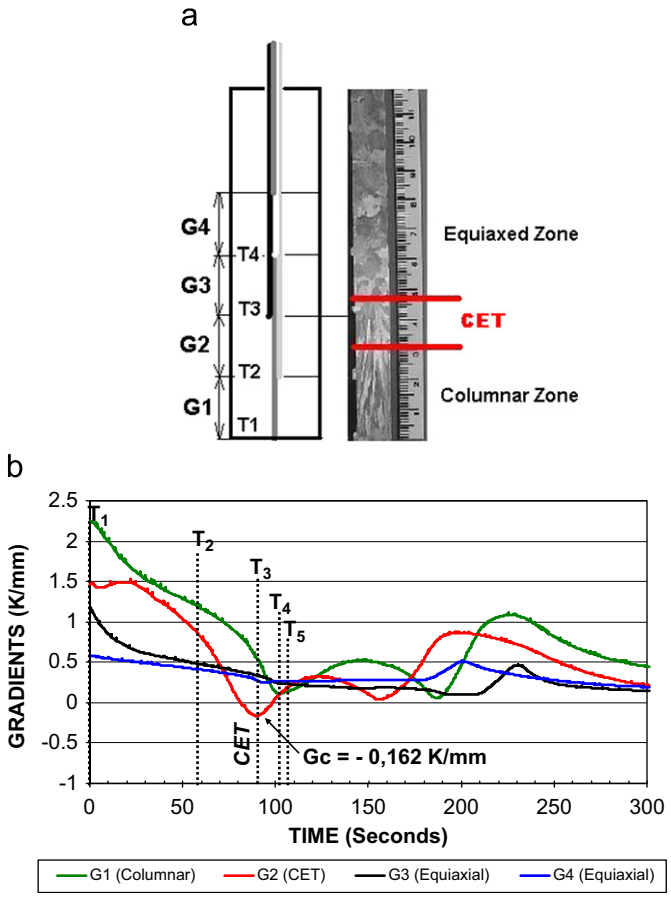

Fig. 3. (a) Scheme of the position of the thermocouples inside the samples during the experiment and positions of the temperature gradients between the thermocouples. (b) Temperature gradient curves versus time. Dashed vertical lines indicate the time at which the liquidus front reaches each thermocouple positions; the line T_1 coincides with the vertical axis and corresponds to the origin of the time axis.

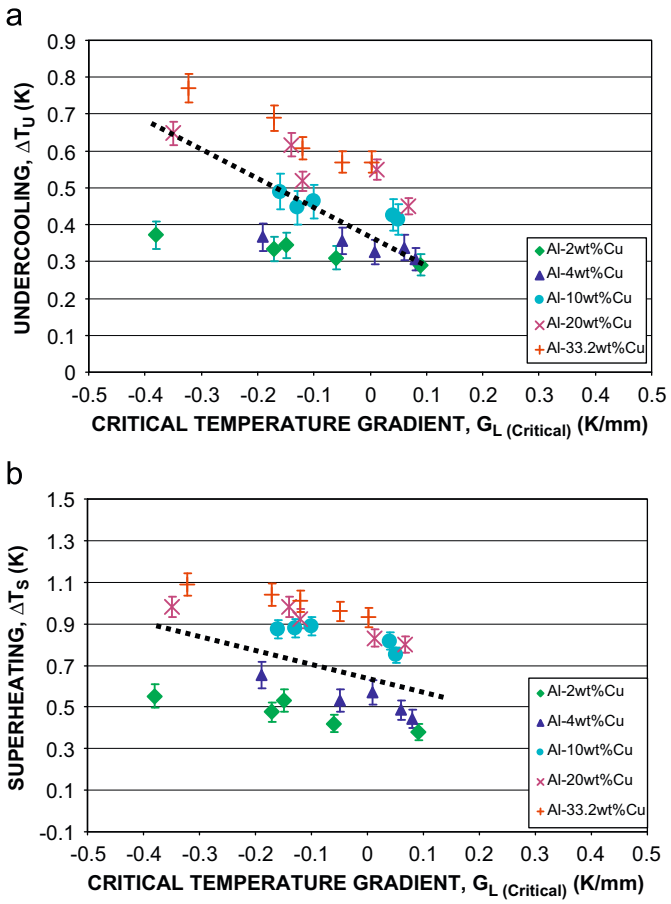

Fig. 4. (a) Undercooling and (b) superheating versus critical temperature gradient.

as 45%. Thereby, taking into account these considerations, it can be concluded that within the error, the alloy composition does not have an effect on the temperature gradient during the transition.

Comparing in Fig. 3(b) the separation in time (x axis) between the dashed vertical lines, which determines the time when the liquidus isotherm (front) reaches the position of the corresponding thermocouple, it is observed that between T_1 and T_2 there are 59.25 s; between T_2 and T_3, 31.39 s; between T_3 and T_4 12.69 s and between T_4 and T_5 only 5.63 s. This shows that first, there is an acceleration of the liquidus interphase and, that the transition occurs not only at a low gradient but also with large interphase velocities.

The variation of undercooling, ΔT_U, and supercooling, ΔT_S, with the critical temperature gradient, $G_{L(Critical)}$, is presented in Fig. 4(a) and (b). It is important to note that both ΔT_U and ΔT_S decrease as $G_{L(Critical)}$ increases. Also, the values of undercooling and superheating are higher when $G_{L(Critical)}$ becomes more negative, especially for Al-20 and Al-33.2 wt%Cu.

3.2.5. *Solidification velocities*

In the present investigation rather than the velocity of the dendrite tips or other interfaces between solid and melt [3] as shown in Fig. 5(a), it is tracked the solid+liquid interphase defined by the liquidus temperature using temperature measurements [28]. It is assumed here that the solid cannot exist beyond the [liquid/(solid+liquid)] interphase and that the liquid cannot exist beyond the [(solid+liquid)/solid] interphase. It is only in the mushy [solid+liquid] zone where all the "interfaces" do exist, and the mushy zone is at temperatures between the local liquidus temperature and the local solid (or eutectic) temperature.

A schematic representation of the position of the liquidus and solidus interphases in an Al–Cu sample during vertical directional solidification with two interphases is presented in Fig. 5(b). A typical result of the position using experimental data of one alloy vertically solidified is showed in Fig. 5(c). These figures show the liquidus interphase and the solidus interphase, which move from the bottom to the top. The solidus interphase departs after the liquidus interphase and usually before this interphase reaches the top of the sample.

The experimental interphase average velocities as a function of distance are shown in Fig. 5(d). It can be noted that after 20 mm the position of the liquidus interphase advances very fast. The solidus front moves well behind the liquidus front at a certain speed and accelerates much less than the liquid after the transition. On the other hand, the velocity of the solidus front remains low. Both velocities are represented in Fig. 5(d). It is observed that, as a result of this, the size of the mushy zone increases very fast. Moreover, there is a specific direction of motion of the interphase which is in the upward direction, thus indicating that heat extraction is from the bottom and that nucleation of new grains after the transition is in a cascade mode rather than in a fully homogeneous nucleation mode.

This pattern was observed in all experiments in which the transition leaves enough equiaxed regions to acquire data for this kind of analysis. The velocity at the instant of the CET, which is equal to 1.8 mm/s, is pointed out in the same figure and is called critical liquidus interphase velocity. The critical values for all the experiments are indicated in Table 2.

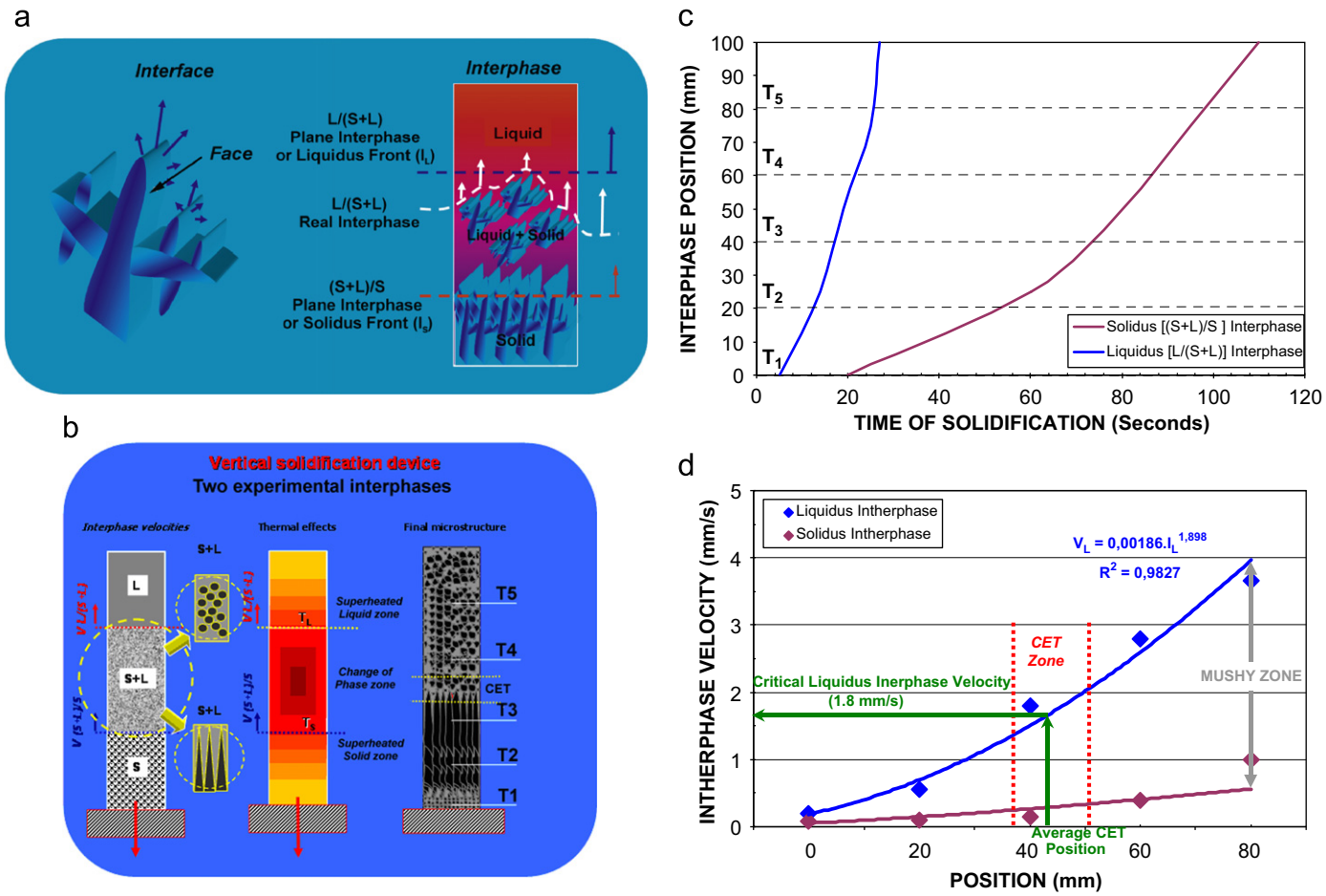

Fig. 5. (a) Scheme showing the dissimilarity between considering interface and interphases. (b) Positions of the liquidus and solidus interphases in Al–Cu samples during vertical directional solidification with two interphases (schematic). (c) Interphase position measured along the sample versus time and (d) interphase velocity measured versus the position along the sample Al-2 wt%Cu alloy.

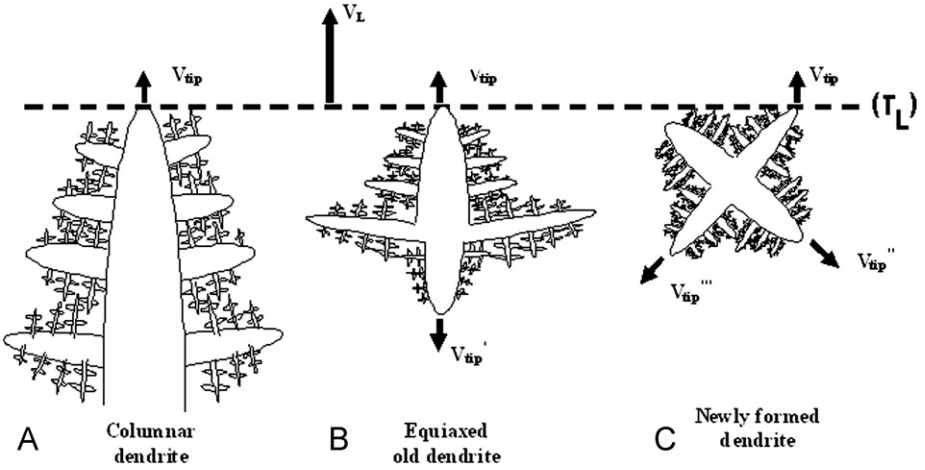

Fig. 6. Schematic showing the type of dendrites formed during the movement of the liquidus interphase from the bottom to the top of the sample. Dendrites type A are present when the growth is columnar, dendrites type A, B or C are present in the CET region and in the fully equiaxed zone only type B and C dendrites coexists.

The values of temperature gradient and liquidus interphase velocity at the instant of the CET were determined and called critical values, $V_{L(Critical)}$ and $G_{L(Critical)}$, respectively (Table 2). These critical values are between 0.67 and 2.16 mm/s for the liquidus interphase velocity and between −0.44 and 0.09 K/mm for the temperature gradient. Other previously reported results about liquidus velocity and temperature gradient at the instant of the CET are between 0.28 and 0.88 mm/s and between 0.28 and 0.75 K/mm, respectively, which are in the order of values reported here [5,25–27]; however, Ziv and Weinberg [13] and Siqueira et al. [7] did not include negative values for the temperature gradient at the CET. The significance of the negative temperature gradient reported here was clearly recognized by Gandin [9,10] in Al–Si alloys and by Ares and Schvezov [18,19] in Pb–Sn and Zn–Al alloys.

The results presented in this report indicate that both the interphase velocity and the temperature gradient are critical parameters associated with the CET. Moreover, in the case of the liquidus interphase velocity, we found that it is possible to establish an average critical value of about 1.48 ± 0.5 mm/s, which is independent of the position of the CET, distance from the chill and alloy composition. It is important to note that the velocity considered here is the velocity of the liquidus isotherm (interphase), which could be different from the tip growth rate (see Fig. 5(a)).

In order to estimate the difference in velocities between the liquidus interphase velocity and the tip growth rate, image sequences taken by Synchrotron X-ray radiographies by Nguyen-Thi et al. [22] and Reinhart et al. [23] were employed. The liquidus interphase velocity is taken as the rate at which the fastest dendrite tip of columnar or equiaxed move. This front of advancing columnar or equiaxed dendrites is nearly flat and it is assumed to have a temperature T_L it is shown in Fig. 6.

During columnar growth where only type A dendrites are present the calculated dendrite tip velocity is 9×10^{-3} mm/s which is very similar to the interphase velocity of 1×10^{-2} mm/s. In such case the columnar dendrites move at a velocity which is about 10% slower than the liquidus interphase velocity.

In the CET region where dendrites type A, B and C coexist the liquidus interphase velocity is 1.6×10^{-2} mm/s and the velocity of the mostly equiaxed dendrite tips is 1.4×10^{-2} mm/s indicating that they are about 14% slower.

Moreover, in the fully equiaxed zone where only type B and C dendrites coexist the calculated liquidus interphase velocity is much faster moving at a speed of 2.2×10^{-2} mm/s. However, the velocity of the tip of the equiaxed dendrites is only 1.4×10^{-2} mm/s or 57% slower than the liquidus interphase velocity.

Fig. 7(a) shows the correlation between the average CET position for each experiment and the values of critical liquidus interphase velocity, and it can be appreciated that the position of the CET increases as the velocity of the critical liquidus interphase increases. Fig. 7(b) shows that the values of the critical temperature gradient become more negative as the critical velocity of the liquidus interphase increases.

3.2.6. *Temperature gradient versus liquidus interphase velocity*

The temperature gradients and the liquidus interphase velocity are calculated and correlated with the type of structure, columnar, CET and equiaxed, present for each pair of values and represented in a standard G_L versus V_L graph.

The result is shown in Fig. 8 where three regions can be defined; a fully equiaxed region for high interphase velocities ($2.4 \le V_L \le 6.4$ mm/s) and low gradients ($0.2 \le G_L \le 2.4$ K/mm), a fully columnar region for large gradients ($1.5 \le G_L \le 9.7$ K/mm) and small velocities ($0.01 \le V_L \le 1.5$ mm/s) and a mixed equiaxed and columnar region separating the other two regions with velocities ($0.67 \le V_L \le 2.16$ mm/s) and gradients ($-0.44 \le G_L \le 0.09$ K/mm).

The Hunt's [12] theory predicts that for temperature gradient in the melt larger than the value given below columnar growth will occur, i.e.

$$G > 0.617(10N_0)^{1/3}\left[1-\left(\frac{\Delta T_N}{\Delta T_C}\right)^3\right]\Delta T_C \quad (1)$$

On the other hand if the gradient is lower than the value given below, equiaxed growth will occur, i.e.

$$G < 0.617N_0^{1/3}\left[1-\left(\frac{\Delta T_N}{\Delta T_C}\right)^3\right]\Delta T_C \quad (2)$$

In order to compare the prediction from this theory with the experimental results obtained in this investigation the following approach was followed. The value of ΔT_c was taken as

$$\Delta T_C = \left(\frac{V' C_0}{A}\right)^{1/2} \quad (3)$$

where A is a constant given by the following equation;

$$A = \frac{1}{4\left(\frac{-2m_L(1-k)\Gamma}{D}\right)} = 300\,\frac{\mu m\%\text{weight}}{sK^2} \text{ for Al–Cu alloys} \quad (4)$$

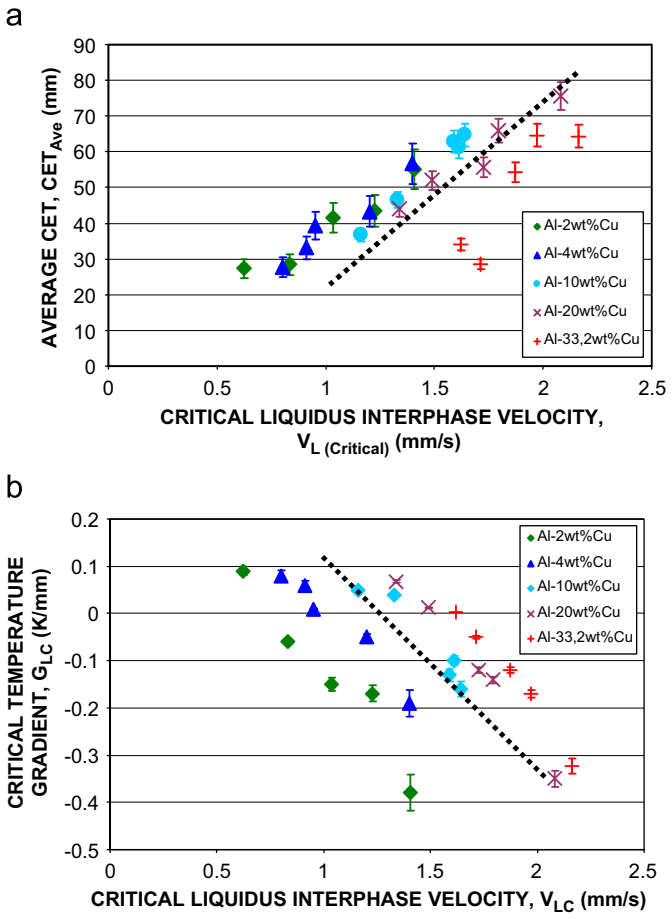

Fig. 7. (a) Average CET position and (b) critical temperature gradient versus critical liquidus interphase velocity.

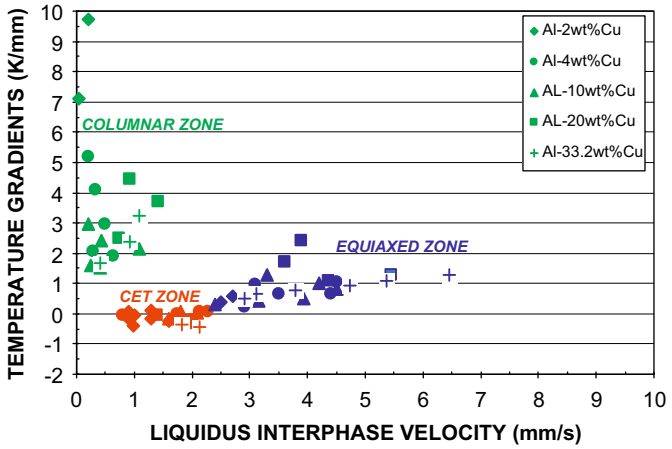

Fig. 8. Temperature gradients in the liquid versus velocity of the liquidus interphase.

Substituting ΔT_c from Eq. (3) into Eqs. (1) and (2) it is possible to obtain two relations between G and V for columnar and equiaxed growth, respectively. Such substitutions leave two parameters ΔT_N and N_0, which are adjusted in such a way as to fit the experimental results. This is done in a graph similar to that of Fig. 8 with the difference that now it is log V versus log G graph constructed for each alloy concentration. In this graph the regions of columnar and equiaxed growths obtained experimentally are identified and Eqs. (1) and (2) are plotted in the same graph, whose position is made to fit the experiments adjusting the values of ΔT_N and N_0. The result for Al-2 wt%Cu is shown in Fig. 9(a) where the two regions are clearly defined (equiaxed and columnar) and the limiting lines given by Eqs. (1) and (2) also clearly separates those fields.

In this case $\Delta T_N = 0.58$ K and $1\ \mathrm{cm}^{-3} > N_0 > 100000\ \mathrm{cm}^{-3}$. First, it is noted that independent of the value of N_0 all the curves converge to a same line for two values of gradient. In addition, it is possible to observe that in the case of Al-2 wt%Cu, the experimental points fit in the correct region; equiaxed or columnar, however, it is not possible to establish which value of N_0 gives the best fit since there are no experimental points near this separation lines. This region corresponds to larger temperature gradients which is not normally present during the experiments.

However, for the alloys with higher copper concentrations the comparison shown in Fig. 9(b–d) shows that the best fit correspond to a value of $N_0 = 100\ \mathrm{cm}^{-3}$. This value of $N_0 = 1000\ \mathrm{cm}^{-3}$ is also the density of grains at the end of solidification and it

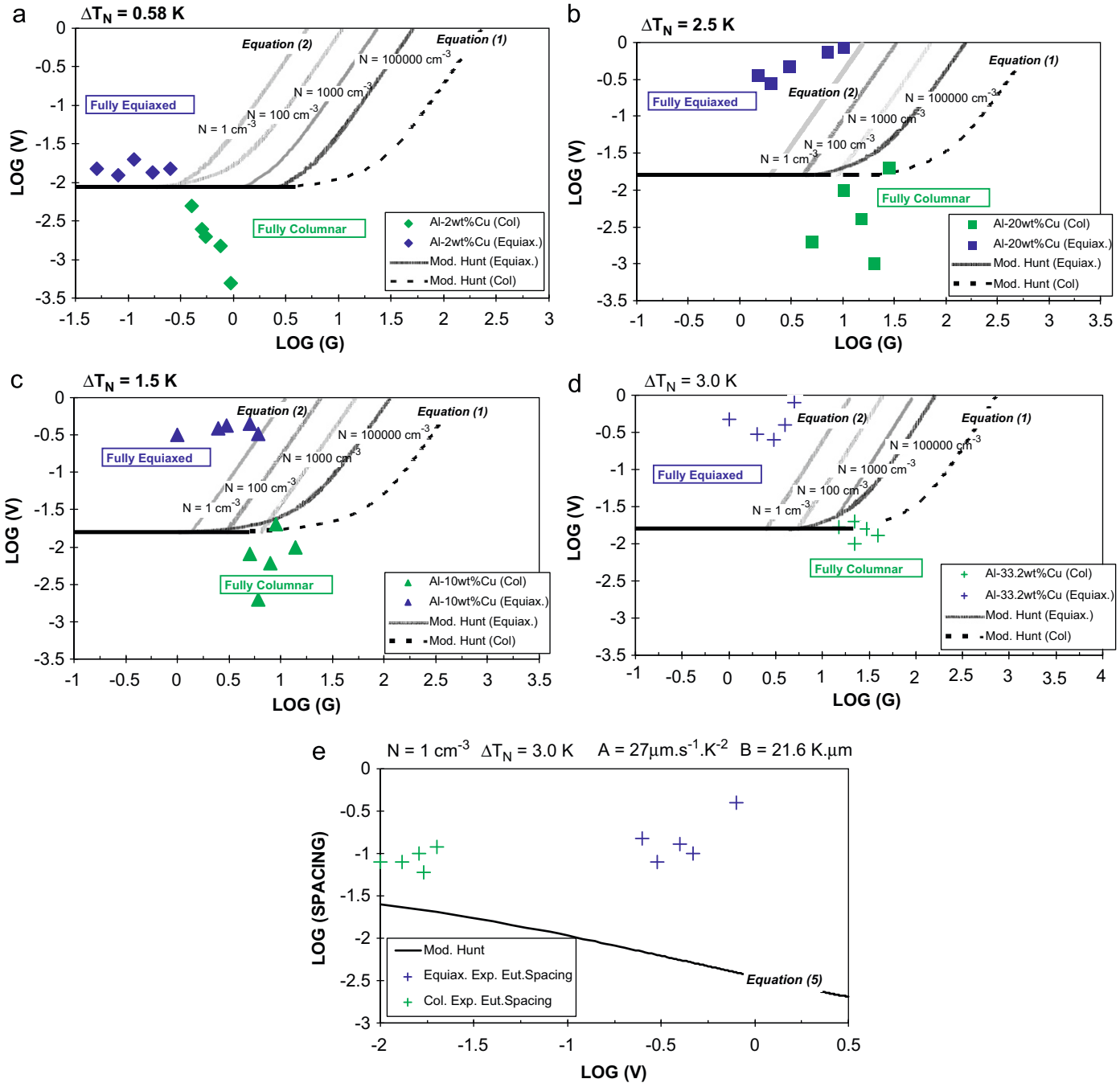

Fig. 9. Graph of log V versus log G with the prediction of Hunt's theory. (a) Al-2 wt%Cu, $\Delta T_N = 0.58$ K, (b) Al-10 wt%Cu, $\Delta T_N = 1.5$ K, (c) Al-20 wt%Cu, $\Delta T_N = 2.5$ K, (d) and (e) Al-33.2 wt%Cu, $\Delta T_N = 3.0$ K.

Table 4
Alloy compositions, average grain sizes, g_s, primary, λ_1, secondary, λ_2, dendritic spacings and eutectic spacings, λ, in each zone of the samples, i.e., columnar zone (CZ), CET zone (CET Z) and equiaxed zone (EZ).

#	Alloy wt%Cu	Average grain size, g_s (mm)				Average primary dendritic spacing, λ_1 (μm)				Average secondary dendritic spacing, λ_2 (μm)			
		Columnar zone	CET zone	Equiaxed zone	Average values in each zone	Columnar zone	CET zone	Equiaxed zone	Average values in each zone	Columnar zone	CET zone	Equiaxed zone	Average values in each zone
1	Al-2wt%Cu	4.05 ± 0.5	1.48 ± 0.3	3.21 ± 0.5	CZ=3.00 ± 0.5	270.22 ± 25	245.21 ± 25	251.23 ± 25	CZ=334.61 ± 36	58.82 ± 5.0	64.12 ± 5.0	74.20 ± 5.0	CZ=66.50 ± 5.0
2		3.14 ± 0.5	1.72 ± 0.3	2.46 ± 0.3	CET Z=1.55 ± 0.3	389.46 ± 36	387.53 ± 36	356.53 ± 36	CET Z=335.77 ± 36	60.96 ± 5.0	69.46 ± 5.0	71.07 ± 5.0	CET Z=72.41 ± 5.0
3		3.04 ± 0.5	1.23 ± 0.3	2.74 ± 0.4	EZ=2.75 ± 0.5	360.22 ± 36	375.69 ± 36	282.80 ± 35	EZ=301.27 ± 36	67.47 ± 5.0	72.08 ± 5.0	68.87 ± 5.0	EZ=68.47 ± 5.0
4		2.55 ± 0.4	1.98 ± 0.4	2.14 ± 0.4		392.53 ± 42	405.13 ± 42	370.11 ± 36		71.68 ± 5.0	76.23 ± 5.0	66.11 ± 5.0	
5		2.25 ± 0.4	1.35 ± 0.3	3.19 ± 0.5		260.61 ± 25	265.28 ± 25	245.68 ± 30		73.56 ± 5.0	80.14 ± 5.0	62.10 ± 5.0	
6	Al-4wt%Cu	3.29 ± 0.5	1.26 ± 0.3	3.37 ± 0.5	CZ=3.78 ± 0.5	347.80 ± 36	284.85 ± 30	257.92 ± 30	CZ=361.67 ± 36	42.11 ± 5.0	62.91 ± 2.0	61.42 ± 4.0	CZ=54.92 ± 5.0
7		3.46 ± 0.5	1.04 ± 0.3	2.47 ± 0.5	CET Z=1.32 ± 0.3	317.26 ± 36	391.50 ± 42	249.27 ± 25	CET Z=353.90 ± 36	48.47 ± 5.0	68.38 ± 4.0	65.20 ± 3.0	CET Z=72.07 ± 5.0
8		3.78 ± 0.5	1.66 ± 0.3	3.15 ± 0.5	EZ=2.97 ± 0.5	358.94 ± 36	330.63 ± 36	287.28 ± 30	EZ=303.94 ± 36	57.58 ± 5.0	72.05 ± 5.0	63.48 ± 5.0	EZ=69.88 ± 5.0
9		4.05 ± 0.5	1.12 ± 0.3	2.83 ± 0.5		373.76 ± 36	317.14 ± 36	305.62 ± 36		58.99 ± 5.0	75.09 ± 5.0	79.17 ± 5.0	
10		4.32 ± 0.5	1.52 ± 0.3	3.03 ± 0.5		410.61 ± 42	445.39 ± 42	419.61 ± 42		67.43 ± 4.5	78.92 ± 5.0	80.12 ± 5.0	
11	Al-10wt%Cu	2.06 ± 0.4	1.35 ± 0.3	2.17 ± 0. 3	CZ=2.37 ± 0.5	257.2 ± 25	298.91 ± 30	221.86 ± 25	CZ=419.14 ± 42	20.72 ± 3.0	41.02 ± 4.5	45.94 ± 5.0	CZ=35.14 ± 4.5
12		2.11 ± 0.4	1.24 ± 0.3	1.72 ± 0. 3	CET Z=1.14 ± 0.3	337.78 ± 36	381.19 ± 35	361.52 ± 36	CET Z=445.77 ± 42	36.32 ± 4.5	46.86 ± 5.0	50.26 ± 5.0	CET Z=48.82 ± 5.0
13		2.38 ± 0.4	1.10 ± 0.3	2.28 ± 0. 3	EZ=1.80 ± 0.5	440.72 ± 42	475.54 ± 42	377.30 ± 36	EZ=337.73 ± 36	36.88 ± 4.5	47.44 ± 5.0	52.50 ± 5.0	EZ=52.26 ± 6.0
14		2.52 ± 0.3	1.06 ± 0.3	1.61 ± 0. 3		520.8 ± 50	523.11 ± 50	415.56 ± 42		38.03 ± 4.5	53.32 ± 5.0	55.11 ± 5.0	
15		2.79 ± 0.3	0.97 ± 0.3	1.25 ± 0. 3		539.2 ± 50	550.12 ± 50	312.41 ± 36		43.76 ± 4.5	55.49 ± 5.0	57.26 ± 5.0	
16	Al-20wt%Cu	1.50 ± 0.4	1.51 ± 0.3	1.55 ± 0. 3	CZ=1.77 ± 0.5	–	–	–	CZ=430.64 ± 42	18.84 ± 3.0	34.12 ± 5.0	25.96 ± 3.0	CZ=29.73 ± 4.0
17		1.62 ± 0.4	1.35 ± 0.3	1.79 ± 0. 3	CET Z=1.29 ± 0.3	425.23 ± 42	443.2 ± 42	226 ± 20	CET Z=429.63 ± 42	25.92 ± 3.0	39.46 ± 5.0	42.50 ± 4.5	CET Z=37.40 ± 4.5
18		1.75 ± 0.4	1.21 ± 0.3	1.25 ± 0. 3	EZ=1.64 ± 0.5	–	–	–	EZ=223.51 ± 20	32.61 ± 4.0	37.08 ± 5.0	52.40 ± 5.0	EZ=42.53 ± 0.5
19		1.96 ± 0.4	1.13 ± 0.3	1.96 ± 0. 3		397.46 ± 42	398.9 ± 36	191.7 ± 20		35.28 ± 4.5	36.23 ± 5.0	46.71 ± 5.0	
20		2.05 ± 0.4	1.29 ± 0.3	1.64 ± 0. 3		469.23 ± 50	446.78 ± 42	252.82 ± 20		36.01 ± 4.5	40.14 ± 5.0	45.09 ± 4.5	

#	Alloy wt%Cu	Average grain size, g_s (mm)				Average eutectic spacing, λ (μm)			
21	Al-33.2wt%Cu	1.25 ± 0.2	1.23 ± 0.3	3.92 ± 0.5	CZ=1.59 ± 0.3	0.05 ± 0.005	0.06 ± 0.005	0.06 ± 0.005	CZ=0.07 ± 0.005
22		1.12 ± 0.2	1.24 ± 0.3	3.26 ± 0.3	CET Z=1.43 ± 0.3	0.04 ± 0.005	0.03 ± 0.005	0.04 ± 0.005	CET Z=0.10 ± 0.005
23		1.52 ± 0.2	1.53 ± 0.3	3.03 ± 0.4	EZ=3.24 ± 0.5	0.08 ± 0.005	0.12 ± 0.005	0.17 ± 0.005	EZ=0.14 ± 0.05
24		1.96 ± 0.3	1.38 ± 0.4	2.74 ± 0.4		0.1 ± 0.05	0.15 ± 0.05	0.25 ± 0.05	
25		2.13 ± 0.3	1.76 ± 0.3	3.27 ± 0.5		0.09 ± 0.05	0.17 ± 0.05	0.19 ± 0.05	

is indicating that during the transition and equiaxed solidification there is no significant melting of grains.

This is supported by the observations due to Nguyen-Thi et al. [22], who sequentially took pictures at different times in Al-3.5%Ni by X-ray radiography in samples 200 μm thick, 40 mm in length and 6 mm in width. The estimated density of grains in this case is in the order of 2000 cm^{-3} and $N_{max}=12{,}500\ cm^{-3}$.

In the special case of the eutectic alloy, the measured spacing of the lamellar structure for equiaxed growth is compared to the prediction given by the Hunt model [12] by means of the following equation:

$$\overline{\lambda}=(1-\phi_c)B(\Delta T_c)^{-1}+\varphi_c.\overline{\lambda}_e \tag{5}$$

where

$\phi_C \approx \frac{4\pi r_C^3 N_0}{3} =$ equiaxed volume fraction, where r_C is the maximum size of the equiaxed grains.

$\Delta T_C=\left(\frac{V}{A}\right)^{1/2}=$ the fraction that is liquid behind the front;

$$\phi_C\overline{\lambda}_e=\int_0^{\varphi_c}\lambda\,d\phi=B'\phi_C\int_0^1(R+A'')^{-1/3}R^2\,dR$$

$$=\frac{3B'\varphi_C}{40}\left\{5(A''+1)^{8/3}-16(A''+1)^{5/3}A''+20A''^2(A''+1)^{2/3}-9A''^{8/3}\right\}$$

$$If\quad A''<<1\Rightarrow\varphi_C.\overline{\lambda}_e=\frac{9\varphi_C B}{8}\left(\frac{3r_C VG}{A}\right)^{-1/3}$$

$$If\quad A''>>1\Rightarrow\frac{\varphi_C B}{\Delta T_N}$$

An average of both is given by Eq. (5), where $B=21.6$ K μm [12].

The results are shown in Fig. 9(e) where it is possible to observe that the experimental points and despite the scattering, are well above the solid line corresponding to the predictions from Eq. (5). The large difference of one order of magnitude could be attributed to the assumptions of steady growth made in the model which is not the case for the present experiments where it has shown a large difference in spacing between the center and the periphery of the grains. The spacing shown in the figure is the average measured spacing in the columnar and equiaxed zones.

3.3. Characterization of the metallographic parameters

3.3.1. Grain size

The results of grain size measurements show that in the transition region the equiaxed grains are small and that after the transition in the equiaxed zone ahead the grain size may have any behavior, that is, increase, decrease or remain constant (see Table 4).

For example, for Al-2wt%Cu, the average grain size in the CET zone is 1.55 mm and in the equiaxed zone 2.75 mm; for Al-4%Cu 1.32 mm in the CET zone and 2.97 mm in the equiaxed zone; for Al-10wt%Cu 1.14 mm in the CET zone and 1.80 mm in the equiaxed zone; for Al-20wt%Cu 1.29 mm in the CET zone and 1.64 mm in the equiaxed zone; and for Al-33.2wt%Cu 1.43 mm in the CET zone and 3.24 mm in the equiaxed zone.

Comparing these results with published results for similar experiments, it is observed that for the same Al-2 wt%Cu alloys, in experiments evolving the transition, similar equiaxed grain sizes have been obtained [7]. However the columnar width reported is about 50% wider. This could be attributed to the larger cooling velocity used in the present investigation, which may affect columnar growth, and, to a larger extent, to the smaller sample size, which reduces convection and as a result produces larger temperature gradients.

3.3.2. Primary dendritic spacing

The average primary and secondary dendritic spacing for each alloy and composition is listed in Table 4 in the columnar, transition and equiaxed regions. The primary spacing is observed to be larger in the columnar and transition regions, where columnar grains co-exist with equiaxed grains, than in the fully equiaxed zone. For instance, for the Al-2 wt%Cu alloy, λ_1 drops from 334 and 335 μm in the columnar and transition regions, respectively, to 301 μm in the equiaxed zone.

Similarly, for the Al-20 wt%Cu alloy, the spacing drops from 430 and 429 μm for the first two zones to 223 μm in the equiaxed zone. In general, the primary spacing reaches a peak value for the columnar grains in the transition zone and then decreases around 30% in the equiaxed region. However, the abrupt change in solidification made from the columnar to the equiaxed zone does not significantly affect the primary spacing. The change from columnar to equiaxed is not only in the solidification mode but also in the solidification time, which increases substantially from the columnar to the equiaxed region.

3.3.3. Secondary dendritic arm spacing

The secondary spacing, λ_2, is larger for the transition and equiaxed zone than for the columnar zone. For the Al-2 wt%Cu alloy, for instance, the spacing is 72 and 68 μm for the transition and equiaxed zones, respectively, and 66 μm for the columnar zone. Similarly, for the Al-20 wt%Cu alloys, the respective values are 37 and 42 μm for the transition and equiaxed zones and 29 μm for the columnar zone. This pattern is repeated for all the concentrations below the eutectic composition (see Table 4).

3.3.4. Eutectic spacing

In the case of the eutectic alloys we showed that the transition from the columnar to the equiaxed zone occurs with characteristics similar to those observed for the other concentrations. The resultant lamellar, rod-like or mixed solidification microstructures have parameters which also depend on solidification conditions, mainly velocity. The measurements show that the average spacings increase from 0.07 μm in the columnar zone to 0.10 μm in the transition region and to 0.14 μm in the equiaxed region, indicating an important reduction in the solidification velocity in this region of the sample (see Table 4).

3.4. Relationship between thermal and structural parameters and it relevance to the CET

3.4.1. Width of columnar grain versus cooling rate

The correlation between the width of the columnar grains and the cooling rate is presented in Table 5 as $W=a\dot{T}^{-b}$, where a and b are fitting parameters; a indicates the standard or absolute reference size for each concentration and b the degree of dependence of width with $\dot{T}$. It is observed that this correlation is larger for lower copper concentrations and decreases as the concentration increases from 4.47 for Al-2 wt%Cu to 2.41 for Al-33 wt%Cu, showing that in general the width decreases as the concentration increases, thus resulting in a structure finer than normally observed. On the other hand, the value of b indicates the sensitivity of width with cooling rate. In all cases the value is less than one with the highest sensitivity at 2 wt%Cu, the lowest sensitivity at 10 wt%Cu, and an increasing sensitivity at 20 wt%Cu.

3.4.2. Primary dendritic spacing versus liquidus interphase velocity and versus cooling rate

The primary spacing as a function of the liquidus interphase velocity for the columnar region where the dendrites grow at a similar rate is shown in Fig. 10 for Al-2 wt%Cu. It is observed that

the spacing decreases with the interphase velocity, following a behavior similar to the predictions of the different theories proposed in the literature by Trivedi [32–34], Kurz and Fisher [35], Hunt [36] and Okamoto and Kishitake [37], However, the predictions differ from the experimental measurements in as much as 50%, being the predictions by Trivedi the closest to the measurements.

The equations proposed by the above-mentioned authors are as follows:

Trivedi [32–34]

$$\lambda_1 = 2\sqrt{2}G^{1/2}V^{1/4}\left[Lk\Delta T_0\Gamma D\right]^{1/4} \quad (6)$$

Kurz and Fisher [35]

$$\lambda_1 = \left[\frac{6\Delta T}{G(1-k)}\left(\frac{D}{V_{TR}} - \frac{\Delta T_0 k}{G}\right)\right]^{1/2} \quad (7)$$

Hunt [36]

$$\lambda_1 = 2\sqrt{2}\left\{D\Gamma\left[m(k-1)\right]C_0\right\}^{1/4}G^{-1/2}V^{-1/4} \quad (8)$$

Okamoto and Kishitake [37]

$$\lambda_1 = 2\varepsilon\left[-DC_0m(1-k)\right]^{1/2}(VG)^{-1/2} \quad (9)$$

The thermophysical data used in the calculation are shown in Table 1 and the meaning of each symbol is indicated at the end of

Table 5
Alloy compositions and expressions for the estimation of width of columnar grains (W), primary (λ_1), secondary (λ_2) dendritic arm spacings and eutectic (λ) spacings in each zone of the samples (columnar, CET and equiaxed) correlating with thermal parameters: cooling rate, $\dot{T}$, liquidus interphase velocity, V_L, and local solidification time, t_{SL}.

Alloy wt%Cu	W versus $\dot{T}$ (mm)	λ_1 versus V_L (μm)	λ_2 versus t_{SL} [38] (μm)	λ_2 versus t_{SL} [39] (μm)	λ_2 versus $\dot{T}$ [40, 41] (μm)
Al-2wt%Cu	$W_{(Col)}=4.47\ \dot{T}^{-0.88}$	$\lambda_1 = 156\,V_{L(Col)}^{-0.096}$ $\lambda_1 = 332\,V_{L(CET)}^{-0.098}$ –	$\lambda_{2(Col)} = 11.9*[t_{SL(Col)}]^{1/3} = 65.9$ $\lambda_{2(CET)} = 11.9*[t_{SL(CET)}]^{1/3} = 71.8$ $\lambda_{2(Equi)} = 11.9*[t_{SL(Equi)}]^{1/3} = 68.4$	$\lambda_{2(Col)} = 10*[t_{SL(Col)}]^{1/2} = 130.4$ $\lambda_{2(CET)} = 10*[t_{SL(CET)}]^{1/2} = 148.3$ $\lambda_{2(Equi)} = 10*[t_{SL(Equi)}]^{1/2} = 137.9$	$\lambda_{2(Col)}=83.6*\dot{T}^{-0.47}=67$ $\lambda_{2(CET)}=89.7*\dot{T}^{-0.41}=74$ $\lambda_{2(Equi)}=91.9*\dot{T}^{-0.58}=70$
Al-4wt%Cu	$W_{(Col)}=4.44\ \dot{T}^{-0.72}$	$\lambda_1 = 167\,V_{L(Col)}^{-0.182}$ $\lambda_1 = 346\,V_{L(CET)}^{-0.196}$ –	$\lambda_{2(Col)} = 11.1*[t_{SL(Col)}]^{1/3} = 53.1$ $\lambda_{2(CET)} = 11.1*[t_{SL(CET)}]^{1/3} = 71.7$ $\lambda_{2(Equi)} = 11.1*[t_{SL(Equi)}]^{1/3} = 69.83$	$\lambda_{2(Col)} = 10*[t_{SL(Col)}]^{1/2} = 105.2$ $\lambda_{2(CET)} = 10*[t_{SL(CET)}]^{1/2} = 164.6$ $\lambda_2 = 10*[t_{SL(Equi)}]^{1/2} = 157.8$	$\lambda_{2(Col)}=88.8*\dot{T}^{-0.74}=60$ $\lambda_{2(CET)}=94.5*\dot{T}^{-0.41}=76$ $\lambda_{2(Equi)}=99.2*\dot{T}^{-0.63}=71$
Al-10wt%Cu	$W_{(Col)}=2.84\ \dot{T}^{-0.37}$	$\lambda_1 = 174\,V_{L(Col)}^{-0.205}$ $\lambda_1 = 462\,V_{L(CET)}^{-0.200}$ –	$\lambda_{2(Col)} = 9.8*[t_{SL(Col)}]^{1/3} = 35.1$ $\lambda_{2(CET)} = 9.8*[t_{SL(CET)}]^{1/3} = 48.8$ $\lambda_{2(Equi)} = 9.8*[t_{SL(Equi)}]^{1/3} = 52.4$	$\lambda_{2(Col)} = 10*[t_{SL(col)}]^{1/2} = 68.2$ $\lambda_{2(CET)} = 10*[t_{SL(CET)}]^{1/2} = 111.3$ $\lambda_2 = 10*[t_{SL(Equi)}]^{1/2} = 123.6$	$\lambda_{2(Col)}=46.2*\dot{T}^{-0.32}=37$ $\lambda_{2(CET)}=77.9*\dot{T}^{-0.64}=50$ $\lambda_{2(Equi)}=88.5*\dot{T}^{-0.74}=53$
Al-20wt%Cu	$W_{(Col)}=2.52\ \dot{T}^{-0.68}$	$\lambda_1 = 205\,V_{L(Col)}^{-0.426}$ $\lambda_1 = 381\,V_{L(CET)}^{-0.456}$ –	$\lambda_{2(Col)} = 8.8*[t_{SL(Col)}]^{1/3} = 29.6$ $\lambda_{2(CET)} = 8.8*[t_{SL(CET)}]^{1/3} = 35.5$ $\lambda_{2(Equi)} = 8.8*[t_{SL(Equi)}]^{1/3} = 42.4$	$\lambda_{2(Col)} = 10*[t_{SL(Col)}]^{1/2} = 61.6$ $\lambda_{2(CET)} = 10*[t_{SL(CET)}]^{1/2} = 81.2$ $\lambda_2 = 10*[t_{SL(Equi)}]^{1/2} = 105.9$	$\lambda_{2(Col)}=49.4*\ \dot{T}-0.63=31$ $\lambda_{2(CET)}=54.4*\ \dot{T}^{-0.52}=37$ $\lambda_{2(Equi)}=54.5*\dot{T}^{-0.32}=43$
Alloy wt%Cu	W versus $\dot{T}$(mm)	λ versus V_L (μm)	λ versus t_{SL} (μm)	λ versus t_{SL} (μm)	λ versus $\dot{T}$ (μm)
Al-33.2wt%Cu	$W_{(Col)}=2.41*\dot{T}^{-0.88}$	$\lambda = 0.06\,V_{L(Col)}^{-0.510}$ $\lambda = 0.10\,V_{L(CET)}^{-0.437}$ $\lambda = 0.23\,V_{L(CET)}^{-0.487}$	$\lambda_{(Col)} = 0.0122*[t_{SL(Col)}]^{1/3} = 0.06$ $\lambda_{(CET)} = 0.0122*[t_{SL(CET)}]^{1/3} = 0.11$ $\lambda_{(Equi)} = 0.0122*[t_{SL(Equi)}]^{1/3} = 0.17$	$\lambda_{(Col)} = 0.010*[t_{SL(Col)}]^{1/2} = 0.12$ $\lambda_{(CET)} = 0.010*[t_{SL(CET)}]^{1/2} = 0.18$ $\lambda = 0.010*[t_{SL(Equi)}]^{1/2} = 0.25$	$\lambda_{(Col)}=0.121*\ \dot{T}^{-0.89}=0.06$ $\lambda_{(CET)}=0.158*\ \dot{T}^{-0.46}=0.11$ $\lambda_{(Equi)}=0.288*\dot{T}^{-0.67}=0.17$

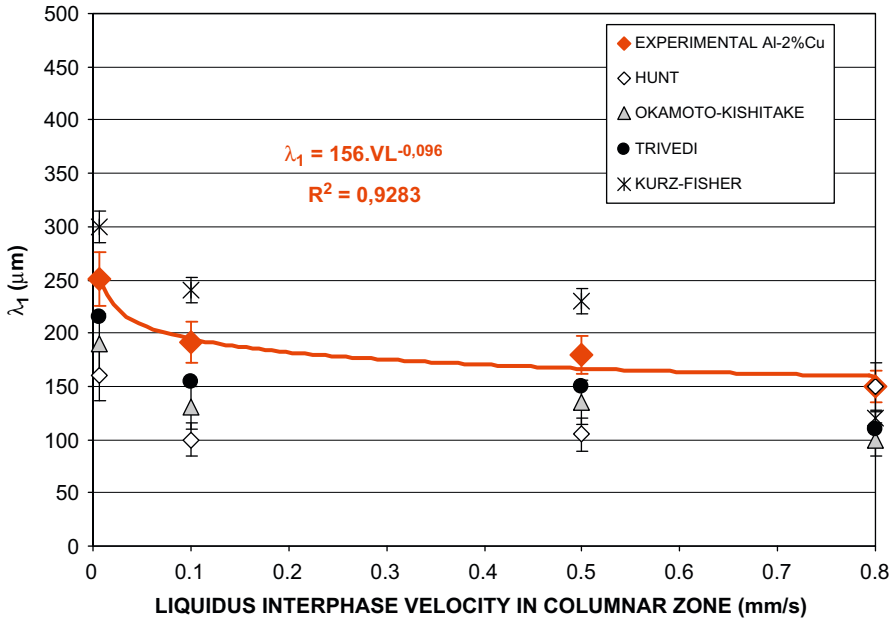

Fig. 10. λ_1 versus liquidus interphase velocity in columnar zone, Al-2 wt%Cu.

the paper (list of symbols). The primary spacing is inversely related to the liquidus interphase velocity in the columnar and the CET zones as $\lambda_1 = a(V_{L(Col)})^{-b}$; such correlation is also calculated and presented in Fig. 10 for Al-2 wt%Cu and in Table 5 for the other three alloys. However, it is observed that the value of a in the columnar zone increases from 156 for Al-2 wt%Cu to 205 for Al-20 wt%Cu, as well as the value of b, changes from 0.096 to 0.42. In the CET zone the value of a increases from 332 for Al-2 wt%Cu to 381 for Al-20 wt%Cu and the values of b changes almost in similar way to the values in the columnar zone.

3.4.3. Secondary dendritic arm spacing and eutectic spacing versus local solidification time

The local solidification time, t_{SL}, at each thermocouple position is determined by the period of time taken by the temperature to go from the liquidus to the solidus temperature.

As it is well established, the secondary spacing, λ_2, is associated with the local solidification time, t_{SL}, quantitatively related to $\lambda_2 \propto t_{LS}^{1/3}$ [38], as a good approximation, or to $t_{LS} \propto \lambda_2^3$. In Table 5 the secondary spacing in equiaxed zone is a function of $t_{LS}^{1/3}$, which is presented with a coefficient adjusted for each alloy within 5% of scatter. It is observed that the coefficient decreases monotonically as the alloy concentration increases from 11.9 for Al-2 wt%Cu to 8.8 for Al-20 wt%Cu, indicating a slightly lower effect of local solidification time with spacing.

It is, therefore, important to point out that there is a very good correlation between λ_2 and $t_{LS}^{1/3}$. However, the correlation proposed by Grugel [39] as $\lambda_2 \propto 10 t_{LS}^{1/2}$ is consequently not as good and the error is around 21%.

Also, Table 5 shows the correlation with the eutectic spacing versus the local solidification time. In this case, there is a better correlation between λ and $t_{LS}^{1/3}$ than between λ and $t_{LS}^{1/2}$.

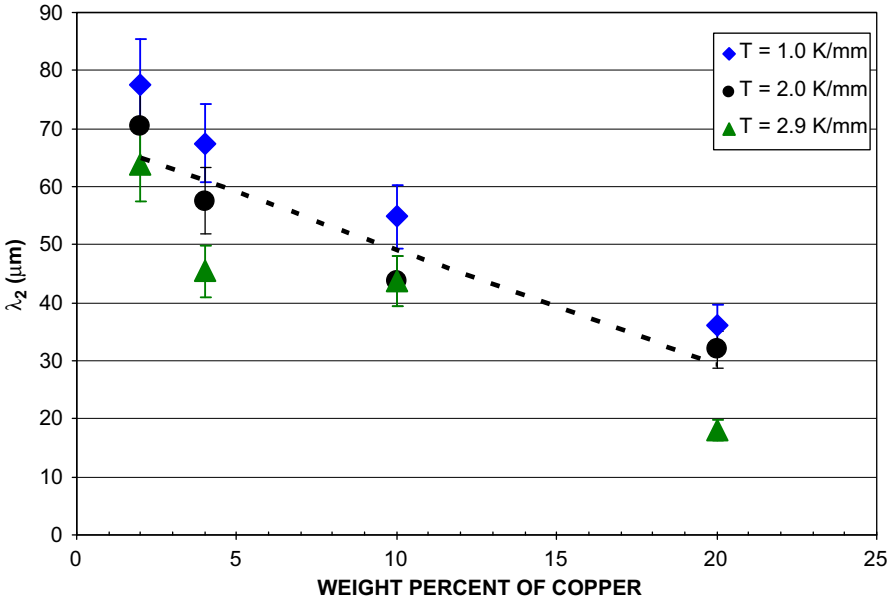

Fig. 11. λ_2 versus weight percent of copper.

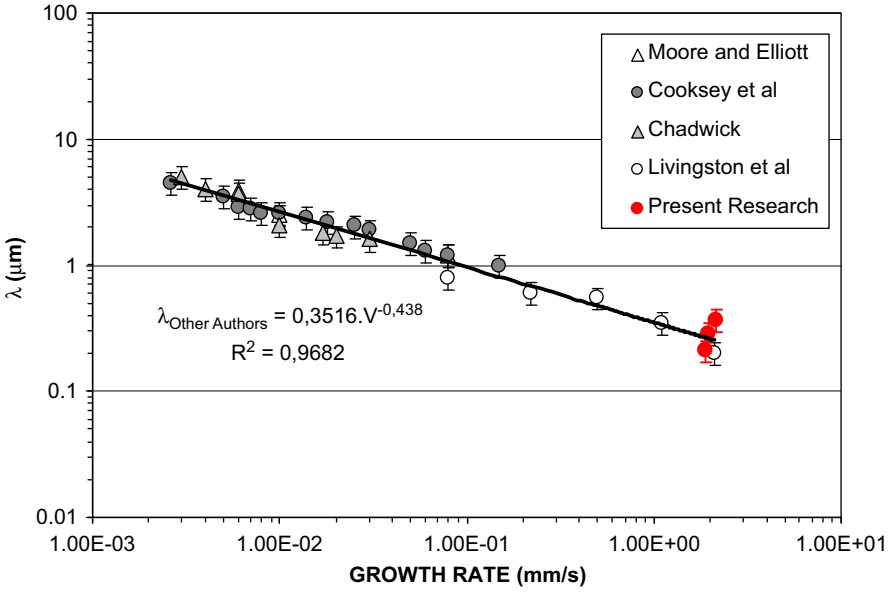

Fig. 12. λ versus growth rate.

As a conclusion, the correlations that best fit the values of λ_2 and λ with t_{LS} are $\lambda_2 \propto t_{LS}^{1/3}$ and $\lambda \propto t_{LS}^{1/3}$, respectively, which can be used to establish the solidification conditions in each region using these relations. An increase of 40% in secondary spacing for the Al-2 wt%Cu alloy from the columnar to the equiaxed transition is the result of an increase of approximately three times in solidification time, or in the case of the Al-20 wt%Cu alloy a 32% increase in λ_2 resulting an increase of 2.3 times in t_{LS}.

3.4.4. Secondary dendritic arm spacing and eutectic spacing versus cooling rate

In addition to the above correlations, it has been proposed [40] that the secondary spacing is inversely related to the cooling rate. Such correlation is also calculated and presented in Table 5 as $\lambda_2 = a(\dot{T})^b$. A value of $a=50$ has been proposed by Jones [41]. However, it is observed that the value of a as well as that of b change from alloy to alloy and with the zone where it is determined, i.e. columnar, CET and equiaxed, showing the limitation to interpret and use this correlation.

Furthermore, the correlation between eutectic spacing, λ and $\dot{T}$, obtaining different expressions and values of constants a and b for each zone of the sample, is presented in the same table.

Fig. 11 shows the effect of the solute content in the secondary dendritic spacing for four Al–Cu alloys solidified with three different cooling rates. It is possible to see that as the Copper content increases, the secondary dendritic spacing decreases for the same cooling rate, $\dot{T}$. In addition, for the same alloy content, as the cooling rate increases the secondary dendritic spacing decreases. These data are consistent with those obtained by Horwarth and Mondolfo [42] in the same alloy system.

3.4.5. Eutectic spacing versus growth rate

The correlation between eutectic spacing and growth rate is presented in Fig. 12 for different experiments extracted from the literature [43–46]. In this figure, the gray and white points correspond to the results obtained by other authors in Al–Cu alloys and the red points correspond to the results obtained in the present research.

The values of λ versus the growth rate obtained by other authors fit the Eq. $\lambda = 0.3516 V_L^{-0.438}$. As mentioned above, it should be noted here that in the present study the critical liquidus interphase velocity, $V_{L(Critical)}$, was correlated with the eutectic spacing, λ; the error in considering the liquidus interphase velocity as a measure of the tip growth rate is less than 15% and it is manifested by the dispersion in the behavior of the red points with respect to the fitting line in Fig. 12. Moreover, expressions corresponding to a correlation of λ versus V_L at the columnar, CET and equiaxed zones are presented in Table 5.

4. Conclusions

The main conclusions of this investigation on the CET in Al–Cu hypoeutectic and eutectic alloys are as follows:

1) The transition in a wide range of Cu concentration between 2 and 33 wt% occurs in a zone rather than in a sharp plane, where both columnar and equiaxed grains in the melt coexist, as previously reported for Pb–Sn and Zn–Al alloys.
2) The transition at the eutectic concentration presents characteristics similar to those for hypoeutectic alloys. The resultant lamellar, rod-like or mixed solidification microstructures have parameters that also depend on the solidification conditions, mainly velocity.
3) From the calculation of thermal parameters, we found that the temperature gradient and the velocity of the liquidus interphase reach critical values at the CET. These critical values are between 0.67 and 2.16 mm/s for the interphase velocity and between -0.44 and 0.09 K/mm for the temperature gradient. Also, the average CET position increases as the liquidus interphase velocity increases. Undercooling and superheating decrease as the temperature gradient at the CET increases. The critical temperature gradient becomes more negative as the critical velocity of the liquidus interphase increases.
4) The measurements of the metallographic parameters show that: (a) in the transition region the equiaxed grains are small and after the transition the grain size may increase, decrease or remain constant. (b) The primary spacing for all Cu concentrations is larger in the columnar and transition zones where columnar grains co-exist with equiaxed grains than in the fully equiaxed zone. The primary spacing reaches a peak value for the columnar grains in the transition zone and then decreases around 30% in the equiaxed region. (c) The secondary spacing is larger for the transition and equiaxed zone than for the columnar zone.
5) Different expressions and values of constants correlating metallographic and thermal parameters were obtained; it is important to note that expressions and constants change from alloy to alloy as well as with the zone where they are determined, i.e., columnar, CET or equiaxed zones.

Acknowledgment

The authors would like to thank CONICET for the financial support.

References

[1] B. Chalmers, in: New York (Ed.), Principles of Solidification, John Wiley & Sons, 1964, p. 123.
[2] S.C. Flood, J.D. Hunt, Metals Handbook, 9th ed., Casting, 15, ASM International, Materials Park, OH, 1989 130.
[3] J.A. Spittle, Columnar to equiaxed grain transition in as solidified alloys, International Materials Reviews 51 (4) (2006) 247–269.
[4] R.T. Southin, Transactions of the Metallurgical Society of Aime 230 (1967) 220–227.
[5] R. Morando, H. Biloni, G.S. Cole, G.F. Bulling, The development of macrostructure in ingots of increasing size, Metallurgical Transactions B (1970) 1407–1412.
[6] V.K. Suri, N. El-Kaddah, J.T. Berry, Transactions of AFS 99 (1991) 187.
[7] C.A. Siqueira, N. Cheung, A. Garcia, Solidification thermal parameters affecting the columnar-to-equiaxed transition, Metallurgical and Materials Transactions 33A (2002) 2107–2117.
[8] C.A. Siqueira, N. Cheung, A. Garcia, The columnar to equiaxed transition during solidification of Sn–Pb alloys, Journal of Alloys and Compounds 351 (2003) 126–134.
[9] Ch.A. Gandin, Experimental study of the transition from constrained to unconstrained growth during directional solidification, ISIJ International 40 (2000) 971–979.
[10] Ch.A. Gandin, From constrained to unconstrained growth during directional solidification, Acta Materialia 48 (2000) 2483–2501.
[11] D.J. Browne, A new equiaxed solidification predictor from a model of columnar growth, ISIJ International 45 (2005) 37–44.
[12] J.D. Hunt, Steady state columnar to equiaxed growth of dendrites and eutectic, Materials Science and Engineering 65 (1984) 75–78.
[13] I. Ziv, F. Weinberg, The columnar-to-equiaxed transition in Al 3 Pct Cu, Metallurgical and Materials Transactions 20A (1989) 731–734.
[14] M. Gäumann, R. Trivedi, W. Kurz, Nucleation ahead of the advancing interface in directional solidification, Materials Science and Engineering A 226–228 (1997) 763–769.
[15] P. Zhu, R.W. Smith, Dynamic simulation of crystal growth by Monte Carlo method, Acta Metallurgica et Materialia 40 (1992) 3369–3379.
[16] S.G.R. Brown, J.A. Spittle, Computer simulation of grain growth and macrostructure development during solidification, Materials Science and Technology 5 (1989) 362–368.
[17] H.B. Dong, P.D. Lee, Simulation of columnar-to-equiaxed transition in directionally solidified Al–Cu alloys, Acta Materialia 53 (2005) 659–668.
[18] A.E. Ares, C.E. Schvezov, Solidification parameters during the columnar-to-equiaxed transition in lead–tin alloys, Metallurgical and Materials Transactions 31A (2000) 1611–1625.

[19] A.E. Ares, C.E. Schvezov, Influence of Solidification Thermal Parameters on the Columnar-to-Equiaxed Transition of Aluminum–Zinc and Zinc–Aluminum Alloys, Metallurgical and Materials Transactions 38A (2007) 1485–1499.
[20] S. McFadden, D.J. Browne, Ch.A. Gandin, A comparison of columnar-to-equiaxed transition prediction methods using simulation of the growing columnar front, Metallurgical and Materials Transactions 40A (2009) 662–672.
[21] R.H. Mathiesen, L. Arnberg, P. Bleuet, A. Somogy, Crystal fragmentation and columnar-to-equiaxed transitions in Al–Cu studied by synchrotron X-ray video microscopy, Metallurgical and Materials Transactions 37A (2006) 2515–2524.
[22] H. Nguyen-Thi, G. Reinhart, N. Mangelinck-Noël, H. Jung, T. Schenk, B. Billia, T. Schenk, J. Gastaldi, J. Härtwig, J. Baruchel, In-situ and real-time investigation of columnar-to-equiaxed transition in metallic alloy, Metallurgical and Materials Transactions A 38A (2007) 1458–1464.
[23] G. Reinhart, H. Nguyen-Thi, N. Mangelinck-Noël, T. Schenk, B. Billia, J. Gastaldi, J. Härtwig, J. Baruchel, In-Situ observation of transition from columnar to equiaxed growth in Al-3.5wt%Ni alloys by synchrotron, modeling of casting, in: Charles-André Gandin, T.M.S. Michel Bellet (Eds.), Welding and Advanced Solidification Processes—XI, The Minerals, Metals & Materials Society, 2006, pp. 359–366.
[24] G.F. Vander Voort, in: Metallography: Principles and Practice, McGraw Hill, 1984, 121.
[25] H.E. Boyer, T.L. Gall, Metals Handbook, Desk Edition. American Society for Metals, Printed in United States of America, Copyright, 1985, 35-18 and 35-35.
[26] M. Vandyoussefi, A.L. Greer, Application of cellular automaton – finite element model to the grain refinement of directionally solidified Al – 4.15 wt% Mg alloys, Acta Materialia 50 (2002) 1693–1705.
[27] M.A. Martorano, C. Beckermann, Ch.A. Gandin, A. Solutal, Interaction mechanism for the columnar-to-equiaxed transition in alloy solidification, Metallurgical and Materials Transactions 34A (2003) 1657–1674.
[28] M.C. Flemings, in: Solidification Processing, McGraw-Hill Series in Materials Science and Engineering, McGraw-Hill, New York, 1974 364.
[29] C.Y. Wang, C. Beckermann, Equiaxed dendritic solidification with convection: Part I. Multiscale/multiphase modelling, Metallurgical and Materials Transactions 27A (1996) 2754–2764.
[30] C.Y. Wang, C. Beckermann, Equiaxed dendritic solidification with convection: Part II, Numerical simulation for an Al-4 wt pct alloy Metallurgical and Materials Transactions 27A (1996) 2765–2783.
[31] C.Y. Wang, C. Beckermann, Equiaxed dendritic solidification with convection: Part III. Comparisons with NH_4Cl–H_2O experiments, Metallurgical and Materials Transactions 27A (1996) 2784–2795.
[32] R. Trivedi, Interdendritic spacing. II: a comparison of theory and experiments, Metallurgical Transactions A 15 (1984) 977–982.
[33] R. Trivedi, Growth of dendritic needles from a supercooled melt, Acta Metallurgica 18 (1970) 287–296.
[34] R. Trivedi, W. Kurz, Solidification microstructures: a conceptual approach, Acta Metallurgica et Materialia 42 (1994) 15–23.
[35] W. Kurz, D.J. Fisher, Dendritic growth and limit of stability tip radius and spacing, Acta Metallurgica 29 (1981) 11–20.
[36] J.D. Hunt, in: Solidification and Casting of Metals, The Metals Society, London, 1979 3–9.
[37] T. Okamoto, K. Kishitake, Dendritic structure in unidirectionally solidified aluminum, tin, and zinc base binary alloys, Journal of Crystal Growth 29 (1975) 137–146.
[38] U. Feurer, in: H. Nieswaag, J.W. Schut (Eds.), Quality Control of Engineering Alloys and the Role of Metals Science, Delft University of Technology, Delft, The Netherlands, 1977, pp. 131–145.
[39] R.N. Grugel, Secondary and tertiary dendrite arm spacing relationships in directional solidified Al–Si alloys, Journal of Materials Science 28 (1993) 677–683.
[40] H. Jones, Microstructure of rapidly solidified materials, Materials Science and Engineering 65 (1984) 145–156.
[41] S.A. Moir, H. Jones, The effect of temperature gradient and growth rate on spacing between primary silicon particles in rapidly solidified hypereutectic aluminium–silicon alloys, Journal of Crystal Growth 113 (1991) 77–82.
[42] J.A. Horwarth, L.F. Mondolfo, Acta Metallurgica 10 (1962) 1037–1042.
[43] A. Moore, R. Elliott, Solidification of metals, Iron and Steels Institute (1969).
[44] D.J.S. Cooksey, D. Munson, M.P. Wilkinson, A. Hellawell, The freezing of some continuous binary eutectic mixtures, Philosophical Magazine 10 (1964) 745–769.
[45] G.A. Chadwick, Monotectic solidification, Journal of Applied Physics 16 (1965) 1095–1097.
[46] J.D. Livingston, H.D. Cline, Monotectic solidification of Cu–Pb alloys [J], Transactions of Metals Society AIME 245 (1969) 351–357.
[47] J.M.V. Quaresma, C.A. Santos, A. Garcia, Correlation between unsteady-state solidification conditions, dendrite spacings, and mechanical properties of Al–Cu alloys, Metallurgical and Materials Transactions 31A (2000) 3167–3178.
[48] J. Lipton, M.E. Glicksman, W. Kurz, Dendritic growth into undercooled alloys melt, Material Science and Engineering 65 (1984) 57–63.
[49] S.E. Kisakurek, An experimental investigation into the formation of an equiaxed zone in ingot casting: Pb–Sb alloy system, Journal of Material Science 19 (1984) 2289–2305.